

Experimental and numerical investigations of nano-additives enhanced paraffin in a shell-and-tube heat exchanger: a comparative study

Zakir Khan ^{a,b}, Zulfiqar Ahmad Khan ^{a*}

^a Bournemouth University, Department of Design & Engineering, NanoCorr, Energy and Modelling (NCEM) Research Group, Fern Barrow, Talbot Campus, Poole, Dorset BH12 5BB, UK.

^b School of Mechanical & Manufacturing Engineering (SMME), National University of Sciences & Technology (NUST), Sector H-12, Islamabad – 44000, Pakistan.

E-mail: zkhan2@bournemouth.ac.uk

Corresponding Author:

^{a*} Bournemouth University, Department of Design & Engineering, NanoCorr, Energy and Modelling (NCEM) Research Group, Fern Barrow, Talbot Campus, Poole, Dorset BH12 5BB, UK.

E-mail: zkhan@bournemouth.ac.uk

Tel.: +44 1202-961645

1 Abstract

2 The impact of metal oxides, metal nitrides and carbon allotropes based nano-additives on
3 thermal conductivity and thermal storage performance of paraffin based latent heat storage
4 (LHS) system is experimentally and numerically investigated. Aluminium oxide (Al_2O_3),
5 aluminium nitride (AIN) and graphene nano-platelets (GnP) based nano-PCM samples are
6 prepared with ultrasonic emulsification technique. Thermal performance enhancements of
7 nano-PCM samples are investigated by conducting a series of charging and discharging
8 experiments in shell-and-tube heat exchanger at various operating conditions. Moreover, a
9 numerical model is developed to account for an impact of varying operating temperature,
10 nano-additives particle size and volume fraction on the effective thermal conductivity and
11 dynamic viscosity of nano-PCM. The numerical model is simulated to investigate the
12 influence of effective thermal conductivity and dynamic viscosity on heat transfer and
13 temperature distribution, phase transition rate and total enthalpy of the system. It is noticed
14 that the charging rates for Al_2O_3 , AIN and GnP based nano-PCM samples are significantly
15 enhanced by 28.01%, 36.47% and 44.57% as compared to pure paraffin, respectively.
16 Likewise, the discharging rates are augmented by 14.63%, 34.95% and 41.46%,
17 respectively. However, the addition of nano-additives compromises the overall thermal
18 storage capacity and augments the effective dynamic viscosity which has adverse impact on
19 natural convection. Therefore, an optimum volume fraction of nano-additives is determined
20 by conducting experimental examinations on Al_2O_3 based nano-PCM samples with volume
21 fraction of 1%, 3% and 5%, at varied operating conditions. It is observed that by increasing
22 volume fraction from 1% to 3%, the charging and discharging rates are significantly
23 enhanced. However, an insignificant enhancement is noticed with further increase in volume
24 fraction from 3% to 5%. Therefore, the optimum volume fraction of 3% is established.
25 Furthermore, GnP based nano-PCM samples have demonstrated higher potential for
26 thermal performance enhancement of LHS system and respective utilisation in practical
27 applications.

28 Keywords

29 Thermal energy storage, Latent heat storage, Phase change materials, Thermal conductivity
30 enhancement, Nano-PCM, Shell-and-tube heat exchanger

Nomenclature

C_p	specific heat capacity at constant pressure (kJ / kg. K)	ρ	density (kg / m ³)
d	diameter (m)	δ_{VF}	volume fraction of nano-additives
F	buoyant force term (N / m ³)	μ	dynamic viscosity (kg / m. s)
g	gravitational acceleration (m / s ²)	φ	fraction of nano-PCM
k	thermal conductivity (W / m. K)	ω	mushy zone constant
k_B	Boltzmann constant		Subscripts
L	latent heat capacity (kJ / kg)	s	solidus phase
M_W	molecular weight	l	liquidus phase
N_A	Avogadro number	pc	phase change
Pr	Prandtl number	np	nano-additives
p	pressure (N / m ²)	pcm	base material
q	heat source term (W / m ³)	$npcm$	nano-PCM
Re	Reynolds number		Acronyms
S	momentum sink term	Al_2O_3	aluminium oxide
T	temperature of nano-PCM (°C)	AlN	aluminium nitride
t	time (s)	GnP	graphene nano-platelets
u	velocity (m / s)	HTF	heat transfer fluid
Greek		LHS	latent heat storage
α	small constant value	PCM	phase change material
β	thermal expansion coefficient (1 / °C)	TES	thermal energy storage

31

32

33 1. Introduction

34 The rapid increase in energy demands to meet world economic developments have
35 escalated dependency on fossil fuels. The energy and fuel crisis along with environmental
36 pollutions and climate change due to extensive usage of fossil fuels to meet industrial and
37 domestic energy demands have raised serious challenges [1, 2]. To mitigate such serious
38 concerns, the development in functional technologies for renewable energy sources or heat
39 recovery systems is imperative to minimise the gap between energy demand and supply.
40 Thermal energy storage (TES) is considered as a decisive technique to store excess thermal
41 energy and utilise it at times to balance energy demand and supply. Latent heat storage
42 (LHS) approach is more attractive category of TES system due to its higher thermal storage
43 capacity and ability to an almost isothermal energy capture and release [3, 4]. LHS system
44 employs phase change materials (PCM) to store and release thermal energy during phase
45 change. LHS systems are integrated with numerous practical applications ranging from solar
46 power plants, waste heat recovery systems, buildings temperature control systems, heating
47 and air conditioning systems, energy balancing and peak shaving management systems,
48 agricultural processing and drying [5-10]. However, due to low thermal conductivity of PCM,
49 the charging and discharging rates of LHS systems are significantly affected, which hinders
50 the widespread practical employability of LHS systems [11, 12]. Therefore, researchers have
51 proposed several techniques to improve overall thermal performance of LHS systems which
52 are: container geometrical orientation, addition of extended surfaces, incorporation of
53 thermal conductive additives and encapsulation techniques [13-18].

54 Shell-and-tube heat exchanger based LHS systems are extensively studied in previous
55 literature due to their better heat transfer performance, minimal thermal losses, design
56 simplicity and easier integration to practical applications. Similarly, extended surfaces are
57 widely adopted for thermal performance enhancement due to their better thermo-physical
58 stability and cost effectiveness. Rathod and Banerjee [19] experimentally investigated the
59 augmentation in charging and discharging rate of stearic acid in shell-and-tube heat
60 exchanger without and with three longitudinal fins. It was informed that the inclusion of
61 longitudinal fins reduced the charging and discharging time by 24.52% and 43.6% as
62 compared to no fins configuration. Likewise, Rabienataj Darzi et al. [20] numerically
63 examined the enhancement in charging and discharging rate of n-eicosane in shell-and-tube
64 heat exchanger with and without longitudinal fins. It was reported that with an increase in
65 number of longitudinal fins from 4 to 20, the melting and solidification rate was enhanced by
66 39-82% and 28-85% as compared to no fins configuration, respectively. Similarly, the phase
67 transition rate and thermal storage capacity of paraffin is numerically examined in a novel
68 geometrical orientation of shell-and-tube heat exchanger with longitudinal fins in [21]. It was
69 discussed that the geometry and material of longitudinal fins had profound impact on
70 charging rate of paraffin. It was reported that with an increase in fins length from 12.7 mm to
71 38.10 mm, the heat transfer was augmented and thus the melting rate was improved by
72 57.32%. Likewise, it was argued that charging rate and thermal storage capacity was
73 improved by 68.8% and 18.06% as the inlet temperature was increased from 50 - 70 °C.
74 Furthermore, this novel design was then developed and connected to flat plate solar
75 collector to conduct experimental studies on charging and discharging cycles [22, 23]. It was
76 noticed that as compared to shell-and-tube heat exchanger without extended fins
77 orientations, the proposed design had displayed relatively higher charging/discharging rate,
78 accumulative thermal energy charge/discharge and mean charge/discharge power. Besides

79 the extended surfaces technique, the inclusion of thermal conductive additives technique is
80 largely acknowledged as an alternate solution to enhance thermal performance with
81 relatively smaller increase in weight of the system.

82 Venkitaraj et al. [24] examined the influence of aluminium oxide (Al_2O_3) nano-particles on
83 thermal performance of pentaerythritol. It was deduced that with an increase in mass fraction
84 of Al_2O_3 from 0.1% to 1%, the effective thermal conductivity was increased from 18.11% to
85 51.79% as compared to pure pentaerythritol. Moreover, the specific heat capacity and latent
86 heat was reported to be decreased from 1.65% to 5.25% and from 1.45% to 4.60%,
87 respectively. Similarly, Tang et al. [25] investigated the thermal performance enhancement
88 of myristic acid with inclusion of Al_2O_3 and graphite nano-particles. It was reported that with
89 an increase in mass fraction from 4% – 12%, the thermal conductivity was improved from
90 0.283 – 0.397 W/m.K for Al_2O_3 and 0.323 – 0.451 W/m.K for graphite based PCM
91 composite. However, the latent heat capacity was recorded to be reduced from 122.87 –
92 109.45 kJ/kg for Al_2O_3 and 112.35 – 88.00 kJ/kg for graphite based composite. Harikrishnan
93 et al. [26] experimented the improvement in thermal conductivity of lauric acid and stearic
94 acid (LA/SA) mixture as base material with dispersion of 1 wt% of TiO_2 , ZnO and CuO nano-
95 particles. It was discussed that the thermal conductivity of LA/SA composite was improved
96 by 34.85%, 46.97% and 62.12%, respectively.

97 Shi et al. [27] reported that thermal conductivity of paraffin was augmented by 10 times with
98 inclusion of 10 wt% of exfoliated graphite nano-platelets. Likewise, Yu et al. [28] inspected
99 the enhancement in thermal performance of paraffin wax with inclusion of short and long
100 multi-walled carbon nanotubes (MWCNT), carbon nanofibers and graphene nano-platelets
101 (GnP). It was discussed that GnP based paraffin composite had elaborated relatively higher
102 thermal conductivity. Likewise, the dynamic viscosity was reported to be increased to 800
103 mPa.s for short/long MWCNT, 40 mPa.s for carbon nanofibers and 11.5 mPa.s for GnP
104 based paraffin composites as compared to 5.892 mPa.s for paraffin wax. Likewise, Fan et al.
105 [29] informed that the thermal conductivity of paraffin is improved by 164% with inclusion of 5
106 wt.% of GnP. Also, Yuan et al. [30] studied the impact of GnP and expanded graphite
107 additives on thermal behaviour of palmitic-stearic acid mixture. It was observed that the
108 thermal conductivity of composites was improved by 2.7 and 15.8 times as compared to
109 base material. However, the latent heat capacity was reduced by 20.90% and 25.17%,
110 respectively.

111 Wang et al. [31] conducted experimental analysis on thermal performance enhancement of
112 polyethylene glycol with aluminium nitride (AIN). It was informed that with an increase in
113 concentration from 5% – 30%, the thermal conductivity of composite was significantly
114 improved from 0.3847 – 0.7661 W/m.K. It was also noticed that inclusion of AIN nano-
115 particles had an insignificant impact on phase transition temperature. Zhang et al. [32]
116 conducted thermal enhancement test on polymethyl methacrylate, polyethylene glycol and
117 AIN nano-particles composite. The concentration of AIN nano-particles was ranged from 5 –
118 30 wt%. It was noticed that thermal conductivity was improved by 7.9% – 53.8%,
119 respectively. However, the latent heat capacity was reduced from 168.5 kJ/kg for
120 polyethylene glycol to 102.5 – 79.2 kJ/kg, respectively. Likewise, Fang et al. [33] reported
121 that the thermal conductivity of paraffin wax was increased from 0.4 – 0.53 W/m.K by
122 inclusion of 10 wt% of boron nitride. Similarly, Yang et al. [34] performed experimental
123 investigation on paraffin and Si_3N_4 based composite. It was reported that thermal

124 conductivity was significantly enhanced by a fraction of 47% for 10 wt% composite.
125 However, the latent heat capacity was observed to be reduced from 186.59 – 113.63 kJ/kg.

126 Arasu and Mujumdar [35] simulated Al₂O₃ nano-particles dispersed in paraffin wax in a
127 square container. It was noticed that as the concentration of nano-additives increased, the
128 dynamic viscosity was augmented which diminishes the impact of increased effective
129 thermal conductivity on melting rate. Therefore, it was concluded that a smaller
130 concentration of nano-additives should be adopted for thermal performance enhancement.
131 Likewise, Mahdi and Nsofor [36] performed numerical examination of Al₂O₃ nano-particles
132 based paraffin in a triplex-tube. It was reported that the solidification time was reduced from
133 8 – 20% as the volumetric concentration was increased from 3 – 8%, respectively. Moreover,
134 Meng and Zhang [37] conducted experimental and numerical investigations on copper foam
135 based paraffin in a rectangular tube in tank orientation. It was discussed that the charging
136 and discharging power was significantly influenced by inlet temperature and flow rate of heat
137 transfer fluid (HTF). Das et al. [38] conducted numerical simulation on n-eicosane and GnP
138 composite in a vertical single tube in shell heat exchanger. It was concluded that for
139 volumetric concentration of 2%, the melting time was shortened by 41% and 37% for inlet
140 temperature of 60 °C and 70 °C, respectively.

141 It can be observed from previous literature that nano-additives based thermal performance
142 enhancement can significantly improve the effective thermal conductivity of nano-PCM;
143 however it will also augment the effective dynamic viscosity and reduce the overall thermal
144 storage capacity. Also, it is noted that the inclusion of metal oxides, metal nitrides and
145 carbon allotropes have presented excellent improvement in thermal conductivity, however
146 the literature lacks a comparatively analysis of these three nano-additives families. It is also
147 identified that the literature lacks an experimental and numerical examination of thermal
148 performance enhancement of nano-PCM in an actual shell-and-tube heat exchanger.
149 Moreover, it is perceived from the literature that the variation in dynamic viscosity with
150 temperature and particle size of nano-additives had not been considered in previous
151 numerical studies [35-38], which had certainly produced erroneous results.

152 This article is focused on the experimental and numerical investigations of metal oxides,
153 metal nitrides and carbon allotropes based thermal performance enhancement of paraffin in
154 a shell-and-tube heat exchanger. Thermal behaviour of nano-PCM samples are examined
155 by conducting a series of charging and discharging cycles in shell-and-tube heat exchanger
156 at various operating conditions. Moreover, this article proposes a numerical model that
157 incorporates the operating temperature, particle size and volumetric concentration of nano-
158 additives while calculating the effective thermal conductivity and dynamic viscosity of nano-
159 PCM. The experimental and numerical studies are focused on identifying the impact of
160 varying effective thermal conductivity and dynamic viscosity of nano-PCM on temperature
161 distribution, liquid fraction, charging/discharging rate and overall enthalpy of the system. The
162 experimental and numerical results discuss the significant enhancement achieved by the
163 three types of nano-additives and identify an optimum volume concentration value to achieve
164 an appropriate thermal performance.

165

166 2. Experimental

167

168 2.1 Materials and Nano-PCM samples preparation

169 In this article, paraffin (RT44HC) is selected as base material for all experimental tests. In
170 order to enhance thermal conductivity of paraffin, three nano-additives are selected which
171 are aluminium oxide (Al_2O_3), aluminium nitride (AIN) and graphene nano-platelets (GnP).
172 The details about materials suppliers and their specifications are listed in **Table 1**. Likewise,
173 the thermo-physical properties of pure paraffin and nano-additives provided by materials
174 suppliers are listed in **Table 2**. The materials are used as received from the dealers without
175 any additional purification.

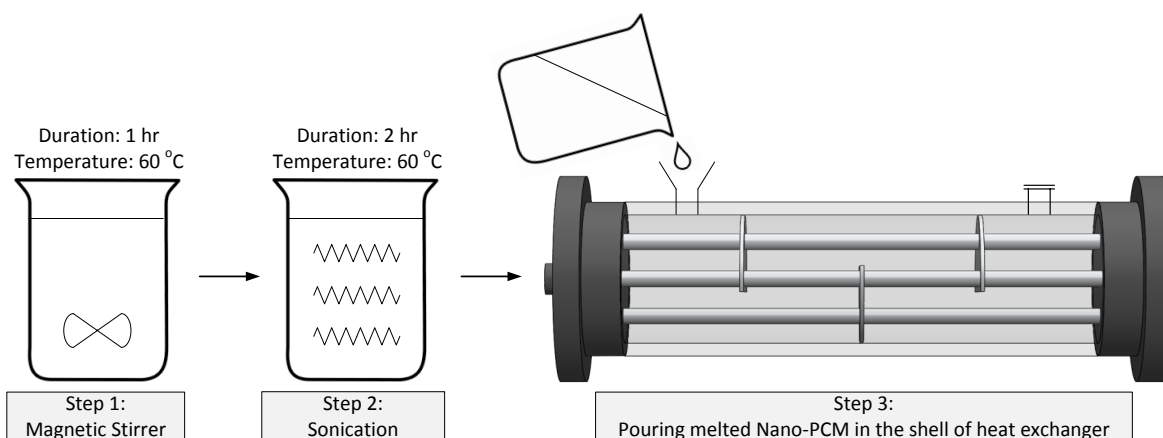
Table 1

List of dealers and specifications of materials used in this study

Materials	Dealers	Particle size	Purity
Paraffin (RT44HC)	Rubitherm Technologies GmbH		99.9%
Al_2O_3	EPRUI Nanoparticles and Microspheres Co. Ltd	30 - 60 nm	99.9%
AIN	Sigma-Aldrich Co. Ltd	<100 nm	99%
GnP	Ionic Liquids Technologies GmbH	6 - 8 nm	99.5%

176

177 The preparation of nano-PCM sample is accomplished by adopting ultrasonic emulsification
178 technique, as shown in **Fig. 1**. In first step, the calculated amount of nano-additive is added
179 to pre-melted base PCM and the suspension is formed by strong agitation using magnetic
180 stirrer for 1 hr. In second step, to achieve complete dispersion of nano-additives in base
181 PCM, the sample is subjected to intensive ultrasonication for 2 hr. In both steps, the
182 temperature of sample is maintained at 60 °C to ensure that the base PCM remains in liquid
183 state. In final step, the nano-PCM sample is poured into the shell of heat exchanger.



184
185

186 **Fig. 1** Schematic illustration of nano-PCM sample preparation and loading in heat exchanger

187 In order to investigate the impact of various nano-additives, a sample for each nano-additive
188 with volume fraction of 1% is prepared. Moreover, three samples of Al_2O_3 based nano-PCM
189 are prepared with volume fraction of 1%, 3% and 5% to examine the influence of increasing
190 volume fraction on thermal performance, as shown in **Table 3**. Prior to investigating nano-
191 PCM in heat exchanger, a sample of pure paraffin is examined to provide a baseline for
192 comparison.

193 The current study is focused on investigating thermal behaviour of nano-PCM samples of
 194 three different nano-additives materials with particle size ranging from 6 nm to 100 nm, as
 195 listed in **Table 1**. As reported in literature [18, 28, 39], an increase in operating temperature
 196 and reduction in particle size could improve the probability and frequency of particles
 197 collisions with base material and could increase interfacial surface area, which would result
 198 in formation of a quasi-convection state. Therefore, the thermal performance of nano-PCM
 199 samples with smaller particle diameter and higher operating temperature would be relatively
 200 higher as compared to larger particle and lower operating temperature. However, the impact
 201 of varying particle sizes of same material on thermal performance of nano-PCM samples are
 202 not investigated in this article.

Table 2
 Thermo-physical properties of pure paraffin and nano-additives

Properties	Paraffin	Al ₂ O ₃	AlN	GnP
Density (kg/m ³)	800 (solid) 700 (liquid)	3500	3300	400
Thermal conductivity (W/m.K)	0.2 (solid) 0.2 (liquid)	36	180	3000
Specific heat capacity (kJ/kg. K)	2.0	0.765	0.74	0.643
Latent heat of fusion (kJ/kg)	255	-	-	-
Phase change temperature (°C)	41-44	-	-	-

203

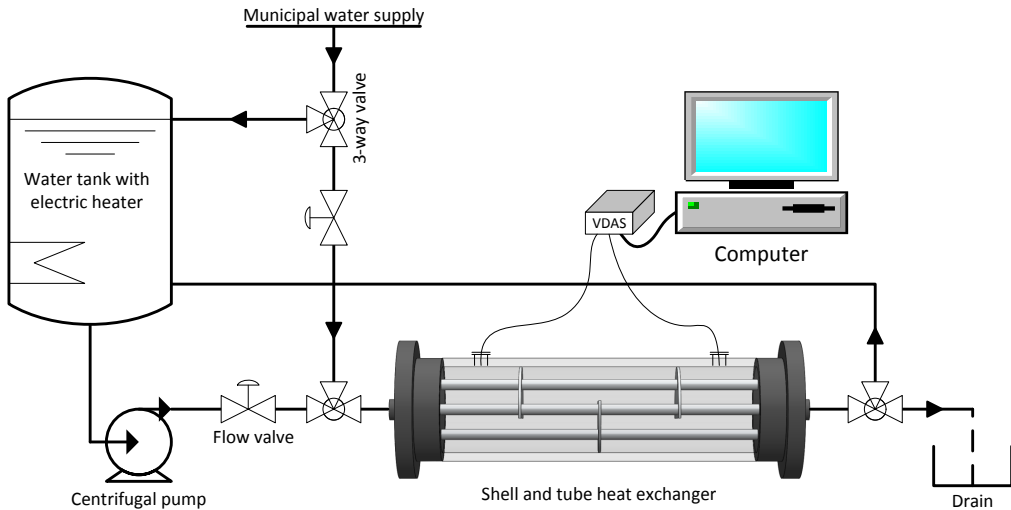
Table 3
 Experimental tests of various nano-PCM samples

Sample	Nano-additives	Volume fraction	Mass of nano-additives added	Mass of paraffin added
A	Al ₂ O ₃	1%	10.61 (g)	207.88 (g)
B	Al ₂ O ₃	3%	32.47 (g)	203.51 (g)
C	Al ₂ O ₃	5%	55.26 (g)	198.95 (g)
D	AlN	1%	10 (g)	207.88 (g)
E	GnP	1%	1.21 (g)	207.88 (g)

204

205 2.2 Experimental setup

206 To investigate thermal behaviour of nano-PCM samples in a heat exchanger, an
 207 experimental setup is developed as shown in **Fig. 2**. The devised system includes water
 208 tank with electric heater, shell-and-tube heat exchanger, centrifugal pump, manual flow
 209 control valves, connections to municipal water and a versatile data acquisition system
 210 (VDAS) with computer.

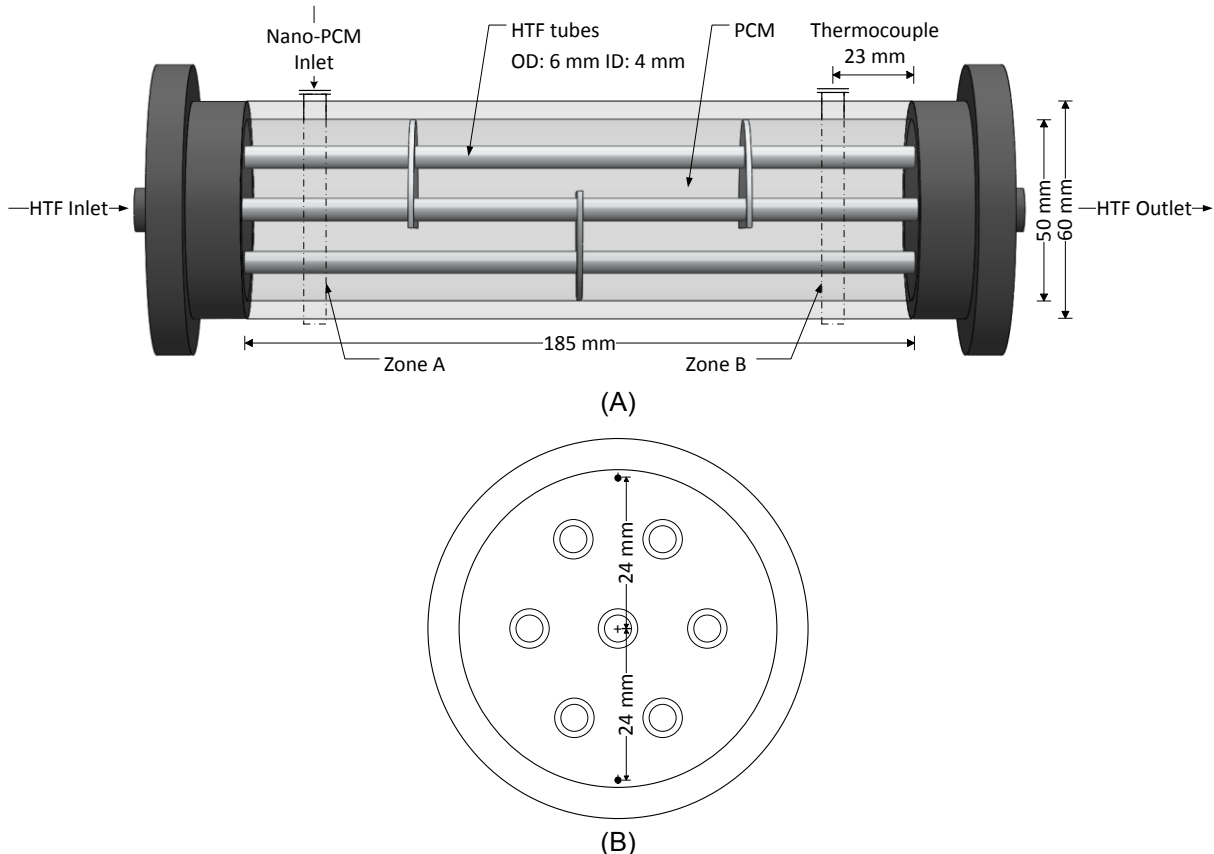


211

212 **Fig. 2** Schematic illustration of experimental setup

213 The electric heater in water tank is governed by digital temperature controller to ensure
 214 constant temperature of HTF during charging cycles. Likewise, centrifugal pump is operated
 215 to direct high temperature HTF from water tank to shell-and-tube heat exchanger. The shell
 216 of heat exchanger is made of acrylic plastic and the outer diameter, length and thickness of
 217 shell are 60 mm, 185 mm and 5 mm, respectively. Similarly, the bundle of seven tubes is
 218 made of stainless steel, with outer diameter and thickness of 6 mm and 1 mm, respectively.
 219 Moreover, the shell-and-tube heat exchanger is insulated with 50 mm thick glass wool to
 220 reduce thermal losses. The insulation layer can be untied to conduct visual inspection of
 221 phase transition process. The shell of heat exchanger is filled with nano-PCM sample and
 222 water as HTF is directed to circulate in the tubes.

223 In order to record transient temperature response of nano-PCM to charging/discharging
 224 cycles, four K-type thermocouples are installed within nano-PCM in the shell. As illustrated in
 225 **Fig. 3 (A)**, two zones are selected to investigate temperature distribution in nano-PCM. The
 226 selected zones are sections close to inlet and outlet regions with a horizontal distance of 23
 227 mm from shell boundaries (both left and right side). Two thermocouples are installed at each
 228 zone, at a vertical distance of \pm 24 mm from central tube, as shown in **Fig. 3 (B)**. Likewise,
 229 two K-type thermocouples are attached to stainless steel tube at inlet and outlet to register
 230 temperature data of HTF. Manual operated flow control valve (turbine flow meter) is installed
 231 at hot/cold circuit each to adjust and record the desired volume flow rate during
 232 charging/discharging cycles. The accuracy values of K-type thermocouples, digital
 233 temperature controller for electric heater and turbine flow meter are \pm 1.5 °C, 0.5% and 3%
 234 of the reading, respectively. To register temperature and flow rate data in computer, VDAS is
 235 operated to transfer data from sensors to computer. VDAS software is used to register
 236 temperature and flow rate reading at time step of 5 s.



237 **Fig. 3** Physical model of shell-and-tube heat exchanger with (A) description of dimensions and (B)
238 vertical positioning of thermocouples at both zone A and B.

239 2.3 Experimental procedure

240 During charging cycles, the low temperature municipal water is initially circulated through the
241 tubes of heat exchanger to provide a good baseline for all charging cycles with initial
242 temperature of 15 °C. The desired temperature is set in digital temperature controller for
243 electric heater to increase temperature of water in tank. Upon reaching the desired
244 temperature, the centrifugal pump is switched on to circulate high temperature HTF through
245 the tubes of heat exchanger. The manual operated flow control valve is adjusted to specific
246 volume flow rate value. In this study, the charging cycles are conducted at three inlet
247 temperatures of 47, 52 and 57 °C and four volume flow rates of 1.5, 2.0, 2.5 and 3.0 l/min for
248 each nano-PCM sample. HTF transfers thermal energy to nano-PCM in heat exchanger and
249 the low temperature HTF at outlet of heat exchanger is directed back to water tank to repeat
250 the cycle. Charging cycle is completed once all thermocouples register temperature value
251 higher than melting temperature of PCM.

252 Prior to conducting discharging cycle, the inlet temperature of HTF is increased to maintain a
253 uniform initial temperature of 50 °C for all discharging cycles. The discharging cycle is
254 started by directing low temperature municipal water to extract thermal energy from nano-
255 PCM. The discharging cycles are examined by regulating flow control valve to a specific flow
256 rate value of 1.5, 2.0, 2.5 and 3.0 l/min. Due to thermal energy discharge to low temperature
257 HTF, the solidification of nano-PCM begins. Discharging cycle is completed once the
258 temperature gradient between inlet temperature and all thermocouples in shell is less than 2
259 °C.

260 3. Numerical Model

261 3.1 Mathematical formulation and governing equations

262 The physical model for numerical investigations is illustrated in Fig. 3. In order to simplify
263 numerical model and shorten simulation time, the following assumptions are made:

- 264 a) The acrylic plastic shell is neglected and the outer boundary is considered as adiabatic
265 by ignoring convective heat losses to surrounding.
- 266 b) The thickness of stainless steel tubes is neglected due to the fact that stainless steel
267 possesses comparatively higher thermal conductivity to nano-PCM.
- 268 c) The liquid phase of nano-PCM is considered as incompressible Newtonian fluid and the
269 change in density with temperature complies with the Boussinesq approximation.
- 270 d) The volumetric expansion of nano-PCM is neglected and natural convection is assumed
271 to be laminar.
- 272 e) The computational domain of nano-PCM is considered to be at uniform initial
273 temperature. Likewise, the inlet temperature and flow rate of HTF are assumed to be
274 constant.

275 Based on above assumptions, a numerical model is formulated considering the governing
276 equations of continuity, momentum and energy to investigate thermal performance of
277 various nano-PCM samples in the computational domain of shell-and-tube heat exchanger.
278 The governing equations are discussed as follow:

279 Continuity equation:

$$\frac{\partial \rho_{npcm}}{\partial t} + \nabla \cdot (\rho_{npcm} \mathbf{u}) = 0 \quad (1)$$

280 Momentum equation:

$$\frac{\partial (\rho_{npcm} \mathbf{u})}{\partial t} + \nabla \cdot (\rho_{npcm} \mathbf{u} \mathbf{u}) = -\nabla p_{npcm} + \nabla \cdot (\mu_{npcm} \nabla \mathbf{u}) + \mathbf{F} + \mathbf{S} \quad (2)$$

281 Energy equation:

$$\frac{\partial (\rho_{npcm} C_p T_{npcm})}{\partial t} + \nabla \cdot (\rho_{npcm} C_p T_{npcm} \mathbf{u}) = \nabla \cdot (k_{npcm} \nabla T_{npcm}) + q \quad (3)$$

282 In Eq. (2), \mathbf{F} represents buoyant force term which is responsible for upward rise of lower
283 density and higher temperature molecules of nano-PCM. Buoyant forces control the natural
284 convection in nano-PCM and it can be approximated by using Boussinesq approximation
285 [40]:

$$\mathbf{F} = \rho_{npcm} \mathbf{g} \beta (T_{npcm} - T_{pc}) \quad (4)$$

286 Likewise, S in Eq. (2) defines momentum sink term which can be estimated by employing
287 KozenyCarman equation, which is derived from Darcy law for porous medium [41]. This term
288 is applied to equate for porosity in mushy zone, as follow:

$$S = \frac{\omega(1-\varphi)^2}{(\varphi^3 + \alpha)} \mathbf{u} \quad (5)$$

289 where ω is the mushy zone constant, which illustrates an approximate magnitude of
 290 damping in governing equation of momentum. In this study, the mushy zone constant value
 291 is set to 10^6 , which presents good agreement between numerical and experimental results.
 292 Likewise, α denotes a small constant value equal to 10^{-4} and is used to prevent division by
 293 zero at liquid fraction $\varphi = 0$. The range of liquid fraction with respect to temperature is
 294 defined as follow:

$$\varphi = \begin{cases} 0 & T_{npcm} < T_s \\ \frac{T_{npcm} - T_s}{T_l - T_s} & T_s \leq T_{npcm} \leq T_l \\ 1 & T_{npcm} > T_l \end{cases} \quad (6)$$

295 where s and l are the indices for solidus and liquidus phase of nano-PCM. The effective
 296 specific heat capacity in Eq. (3) is calculated by differentiating specific enthalpy with respect
 297 to temperature:

$$C_p = \frac{1}{\rho} (\varphi_s \rho_{npcm,s} C_{p,npcm,s} + \varphi_l \rho_{npcm,l} C_{p,npcm,l}) + L_{npcm} \frac{\partial}{\partial T} \left[\frac{(\varphi_l \rho_{npcm,l} - \varphi_s \rho_{npcm,s})}{2\rho_{npcm}} \right] \quad (7)$$

298 The right hand side of Eq. (7) represents that specific heat capacity is the summation of
 299 sensible and latent portion of heat. Likewise, the thermo-physical properties of nano-PCM
 300 are estimated based on theoretical equations for mixture of two components, as follow [42]:

$$\rho_{npcm} = \delta_{VF} \rho_{np} + (1 - \delta_{VF}) \rho_{pcm} \quad (8)$$

$$C_{p,npcm} = \frac{\delta_{VF} \rho_{np} C_{p,np} + (1 - \delta_{VF}) \rho_{pcm} C_{p,pcm}}{\rho_{npcm}} \quad (9)$$

$$L_{npcm} = \frac{(1 - \delta_{VF}) \rho_{pcm} L_{pcm}}{\rho_{npcm}} \quad (10)$$

301 where δ_{VF} represents the volume fraction of nano-additives. Moreover, the effective dynamic
 302 viscosity and effective thermal conductivity of nano-PCM samples are evaluated by
 303 implementing the semi-empirical models proposed by Corcione [43] as given in Eq. (11) and
 304 Eq. (14), respectively. These propose models by Corcione, on contrary to earlier standard
 305 models and theories proposed by Einstein [44] and others [45-48] for estimating the effective
 306 dynamic viscosity and Maxwell [49] and others [50-52] for approximating the effective
 307 thermal conductivity, account for particle size of nano-additives, volume fraction and
 308 operating temperature. Therefore, these earlier standard models fail to predict an accurate
 309 increase in dynamic viscosity and thermal conductivity of nano-PCM due to the fact that
 310 these standard models are developed for larger particle size nano-additives and these
 311 models only depend on shape and volume fraction of nano-additives.

312 The effective dynamic viscosity is estimated as follow [43]:

$$\mu_{npcm} = \frac{\mu_{pcm}}{1 - 34.87(d_{np}/d_{pcm})^{-0.3} \delta_{VF}^{1.03}} \quad (11)$$

313 where μ_{pcm} , d_{pcm} and d_{np} represents the dynamic viscosity of pure paraffin, equivalent
 314 diameter of pure paraffin and diameter of nano-additives, respectively. The dynamic
 315 viscosity [53] and equivalent diameter of pure paraffin [43] are determined as follow:

$$\mu_{pcm} = 0.001 \exp\left(-4.25 + \frac{1790}{T_{pcm}}\right) \quad (12)$$

$$d_{pcm} = 0.1 \left(\frac{6M_W}{\pi N_A \rho_{pcm,o}} \right)^{1/3} \quad (13)$$

316 where M_W , N_A and $\rho_{pcm,o}$ are the molecular weight of pure paraffin, Avogadro number and
 317 density of pure paraffin at $T_{pcm} = 20^\circ\text{C}$, respectively.

318 Similarly, the effective thermal conductivity is evaluated from the following equation [43]:

$$k_{nPCM} = k_{PCM} \left(1 + 4.4 Re^{0.4} Pr^{0.66} \left(\frac{T_{nPCM}}{T_{PC}} \right)^{10} \left(\frac{k_{np}}{k_{PCM}} \right)^{0.03} \delta_{VF}^{0.66} \right) \quad (14)$$

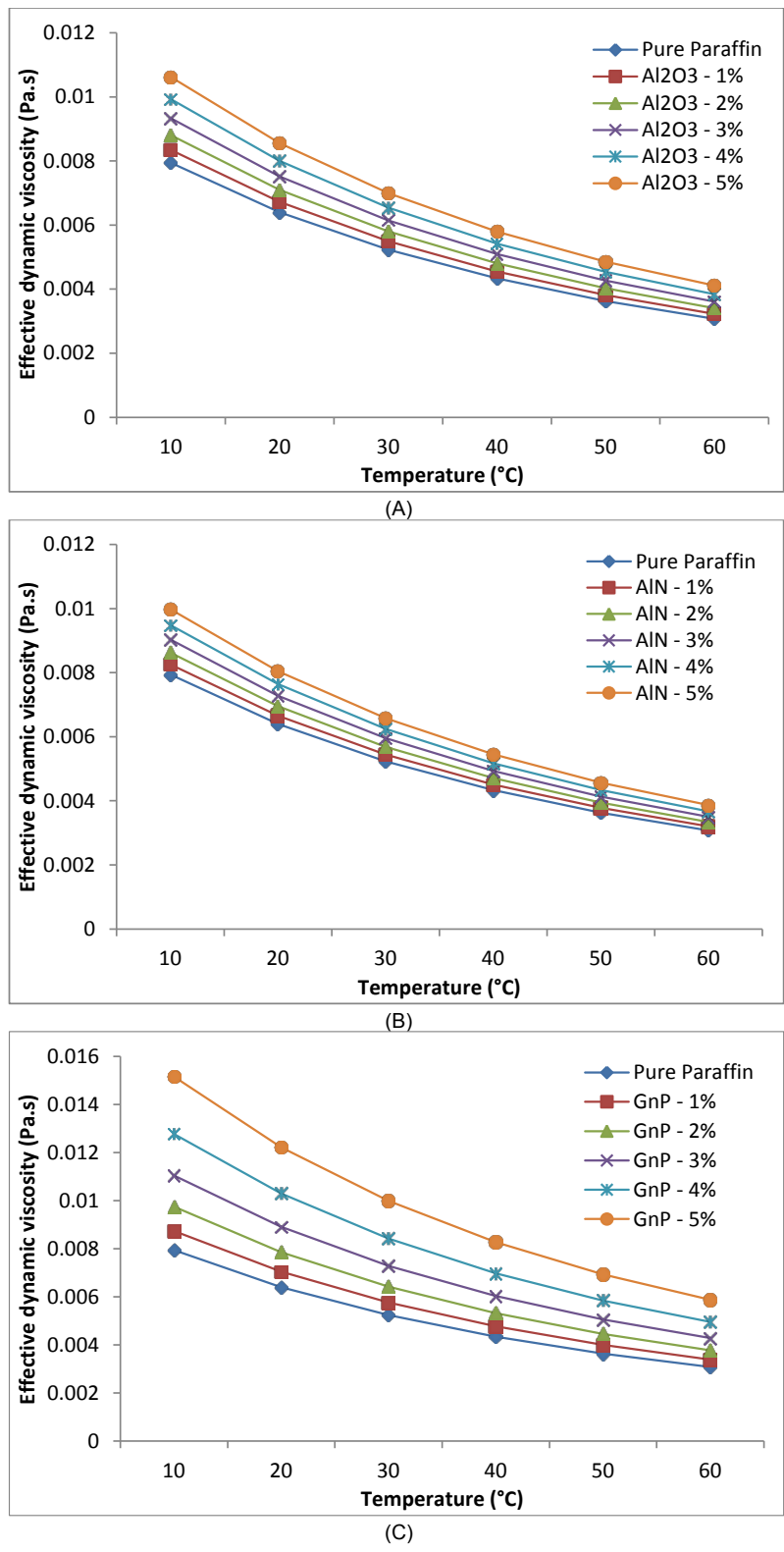
319 where Re and Pr represent the Reynolds number of nano-additives and Prandtl number of
 320 pure paraffin, respectively. Re and Pr can be calculated using the following relations [43]:

$$Re = \frac{2\rho_{PCM} k_B T_{nPCM}}{\pi \mu_{PCM}^2 d_{np}} \quad (15)$$

$$Pr = \frac{\mu_{PCM} C_{p,PCM}}{k_{PCM}} \quad (16)$$

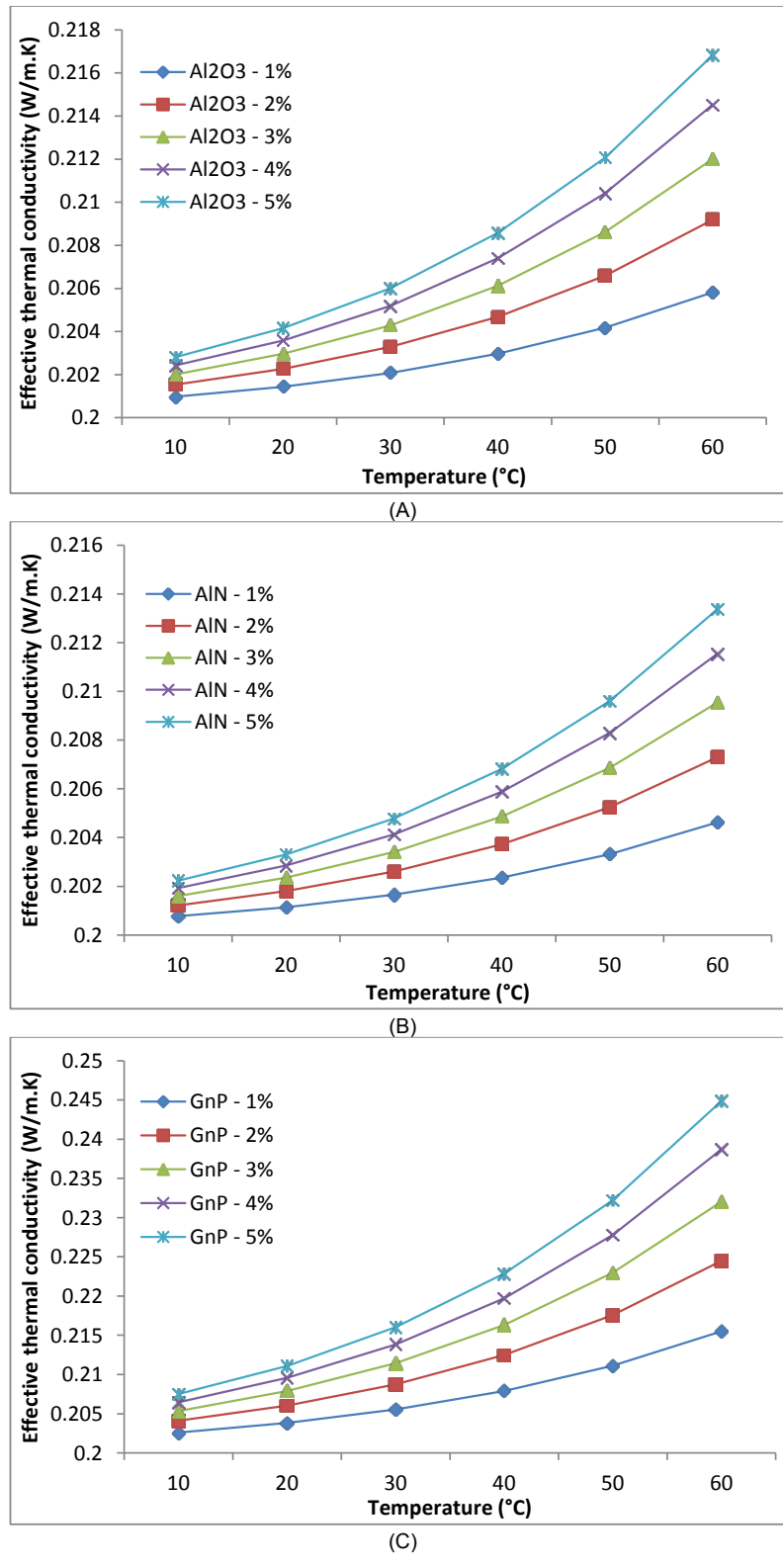
321 Using Eq. (11) and Eq. (14), the effective dynamic viscosity and thermal conductivity of
 322 nano-PCM are computed for volume fraction of 1%, 2%, 3%, 4% and 5% of Al_2O_3 , AlN and
 323 GnP nano-additives, as presented in **Fig. 4** and **Fig. 5**, respectively. It can be noticed that in
 324 all cases, the dynamic viscosity of nano-PCM as compared to pure paraffin is enhanced with
 325 an increase in volume fraction of nano-additives. However, the enhancement in effective
 326 dynamic viscosity of GnP based nano-PCM is more significant as compared to Al_2O_3 and
 327 AlN based nano-PCM. This is due to the fact that the effective dynamic viscosity is highly
 328 influenced by the particle size and shape of nano-additives. Moreover, a higher dynamic
 329 viscosity can have an adverse impact on natural convection.

330 Likewise, the enhancements in thermal conductivity of nano-PCM due to varied volume
 331 fraction concentration of nano-additives are illustrated against temperature in **Fig. 5**. It can
 332 be observed that GnP based nano-PCM samples have shown significantly higher thermal
 333 conductivity due to their smaller particle size and higher thermal conductivity as compared to
 334 Al_2O_3 and AlN.



335

336 **Fig. 4** Effective dynamic viscosity of nano-PCM samples with varied volume fractions and nano-
 337 additives (A) Al₂O₃, (B) AlN and (C) GnP.



338

339 **Fig. 5** Effective thermal conductivity of nano-PCM samples with varied volume fractions and nano-
 340 additives (A) Al₂O₃, (B) AlN and (C) GnP.

341 3.2 Initial and boundary conditions

342 During melting process, the initial temperature of nano-PCM is set to 15 °C which is less
 343 than phase change temperature, as shown in **Table 2**. Therefore, the initial temperature

344 ensures that entire mass of nano-PCM is in complete solid state. Likewise, the HTF tubes
 345 are set to a constant inlet temperature of 52 °C for the complete charging cycle.

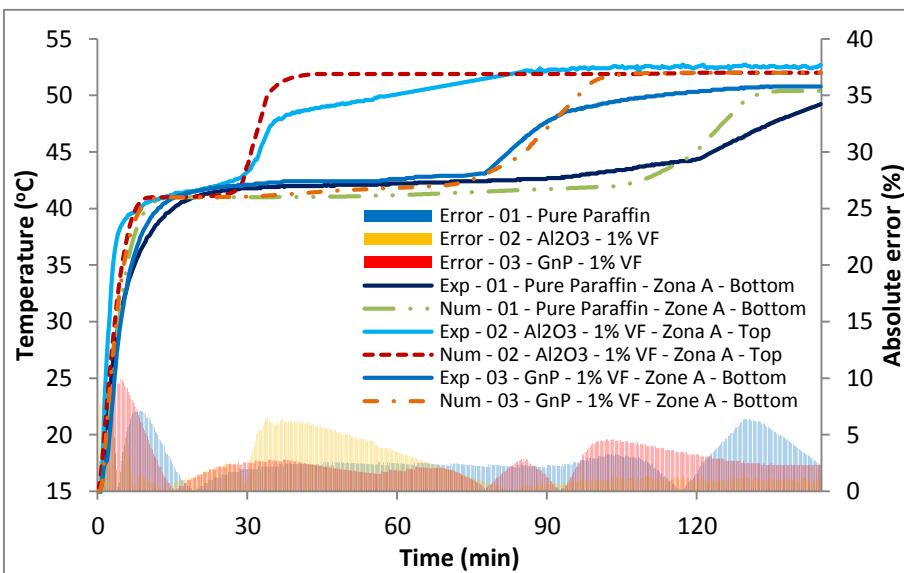
346 3.3 Computational procedure and model validation

347 The geometrical orientation and dimensions of shell-and-tube heat exchanger provided in
 348 **Fig. 3** are adopted for the computational model. The governing equations are discretised by
 349 implementing finite volume method. PISO algorithm is employed to solve the pressure-
 350 velocity coupling. PRESTO and second order upwind schemes are adopted for spatial
 351 discretisation of pressure, momentum and energy equations, respectively. The relative
 352 residuals values for the convergence criteria of continuity, velocity and energy equations are
 353 set to 10^{-6} , respectively. The time step and mesh size independency study are conducted on
 354 nano-PCM sample A (see **Table 3**) to ensure accuracy of numerical results, as presented in
 355 **Table 4**. As a result, the time step of 1 s and mesh size of 27420 are selected for all nano-
 356 PCM samples in this study. In order to validate the computational model with experimental
 357 results, the transient temperature profiles for three nano-PCM samples are acquired from
 358 numerical and experimental procedures for conducting charging cycles at constant inlet
 359 temperature of 52 °C, which are compared and plotted in **Fig. 6**. The set of three samples
 360 include pure paraffin, Al₂O₃ and GnP based nano-PCM samples with 1% volume fraction,
 361 respectively. The mean absolute percentage error between numerical and experimental
 362 results for pure paraffin and nano-PCM samples are computed to be 2.87%, 2.53% and
 363 2.75%, respectively.

Table 4

Mesh size and time stepping independency conducted on sample A (Al₂O₃ – 1% VF)

Case	Inlet temperature (°C)	Mesh element size	Time step (s)	Total melting time (min)	Percent error (%)
I	52	6930	1	98	6.81
II	52	27420	1	91.75	-
III	52	43585	1	91.5	0.27
IV	52	27420	0.1	91.25	0.54
V	52	27420	0.5	91.5	0.27



364
 365 **Fig. 6** Validation of experimental and numerical results by comparing temperature profiles and
 366 respective absolute percentage error while charging at inlet temperature of 52 °C.

367 4. Results and discussions

368 4.1 Thermal performance of pure paraffin

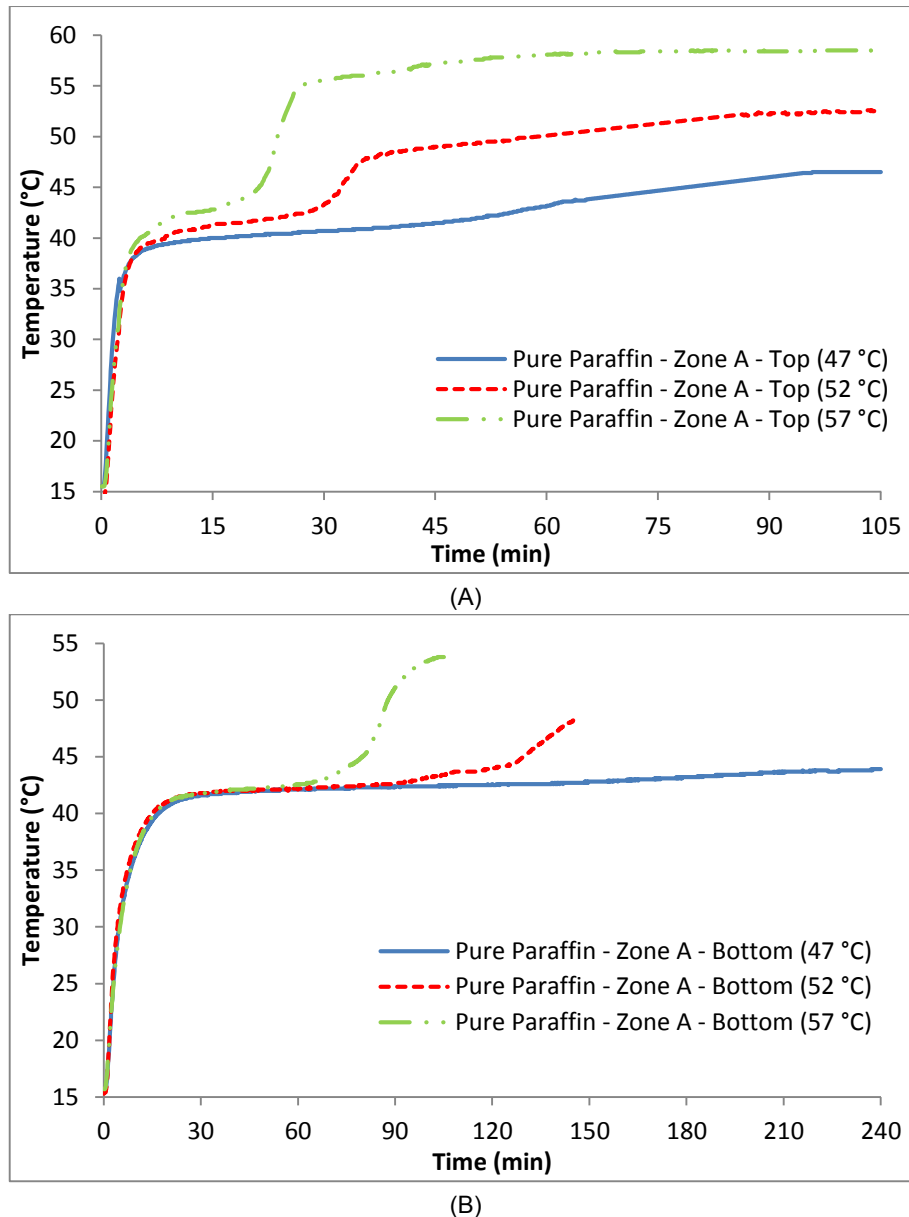
369 In order to understand the thermal performance of nano-PCM samples in shell-and-tube
370 heat exchanger, a sample of pure paraffin is initially examined to develop a good baseline
371 for comparison.

372 4.1.1 Experimental

373 Pure paraffin sample is melted and poured in the shell of heat exchanger. In order to study
374 the transient thermal response of pure paraffin to various inlet temperatures and volume flow
375 rates of HTF, the data is registered from all four k-type thermocouples installed at zone A
376 and B, as presented in **Fig. 3**. The temperature distribution in both vertical and horizontal
377 positions in shell is examined at three inlet temperatures of 47, 52 and 57 °C. Likewise, the
378 impact of varying flow rate of HTF is studied at four values of 1.5, 2.0, 2.5 and 3.0 l/min.

379 The melting behaviour of pure paraffin at various temperatures is presented in **Fig. 7**. It can
380 be noticed that the linear rise from initial temperature to about 40 °C represents sensible
381 heat and it is dominated by conduction heat transfer. The sensible heat capacity is rapidly
382 stored due to small specific heat capacity of paraffin. Afterwards, a steady and gradual rise
383 is observed, which represents the latent portion of heat storage. During this phase, the
384 higher latent heat capacity is gradually stored as the temperature rises from 41 °C to 44 °C.
385 Consequently, the phase transformation of solid paraffin to mushy and then to liquid state
386 occurs. After completion of latent portion of heat storage, a relatively quicker increase in
387 temperature is observed which again represent the sensible heat storage in liquid phase of
388 paraffin.

389 Moreover, it can be observed from **Fig. 7** that phase transition at top position is quicker as
390 compared to bottom position. The reason behind is that conduction dominates the heat
391 transfer at initial stages and after phase transition; the amount of liquid paraffin increases
392 which results into upward rise against the gravity and thus it makes natural convection as
393 dominant mode of heat transfer. Due to upward rise of high temperature molecules, the
394 phase transition is relatively higher at top position as compared to bottom position. The
395 natural convection is highly influenced by density and dynamic viscosity. Moreover, it can be
396 noticed that with an increase in inlet temperature of HTF, the temperature gradient for heat
397 transfer increases which results in relatively higher melting/charging rate of paraffin. Also,
398 due to small volume capacity of shell-and-tube heat exchanger, the varying volume flow rate
399 of HTF has insignificant influence on phase transition rate. It is noticed that with an increase
400 in volume flow rate from 1.5 to 3.0 l/min, an almost identical transient temperature response
401 is recorded with a relative standard deviation of 0.43%.

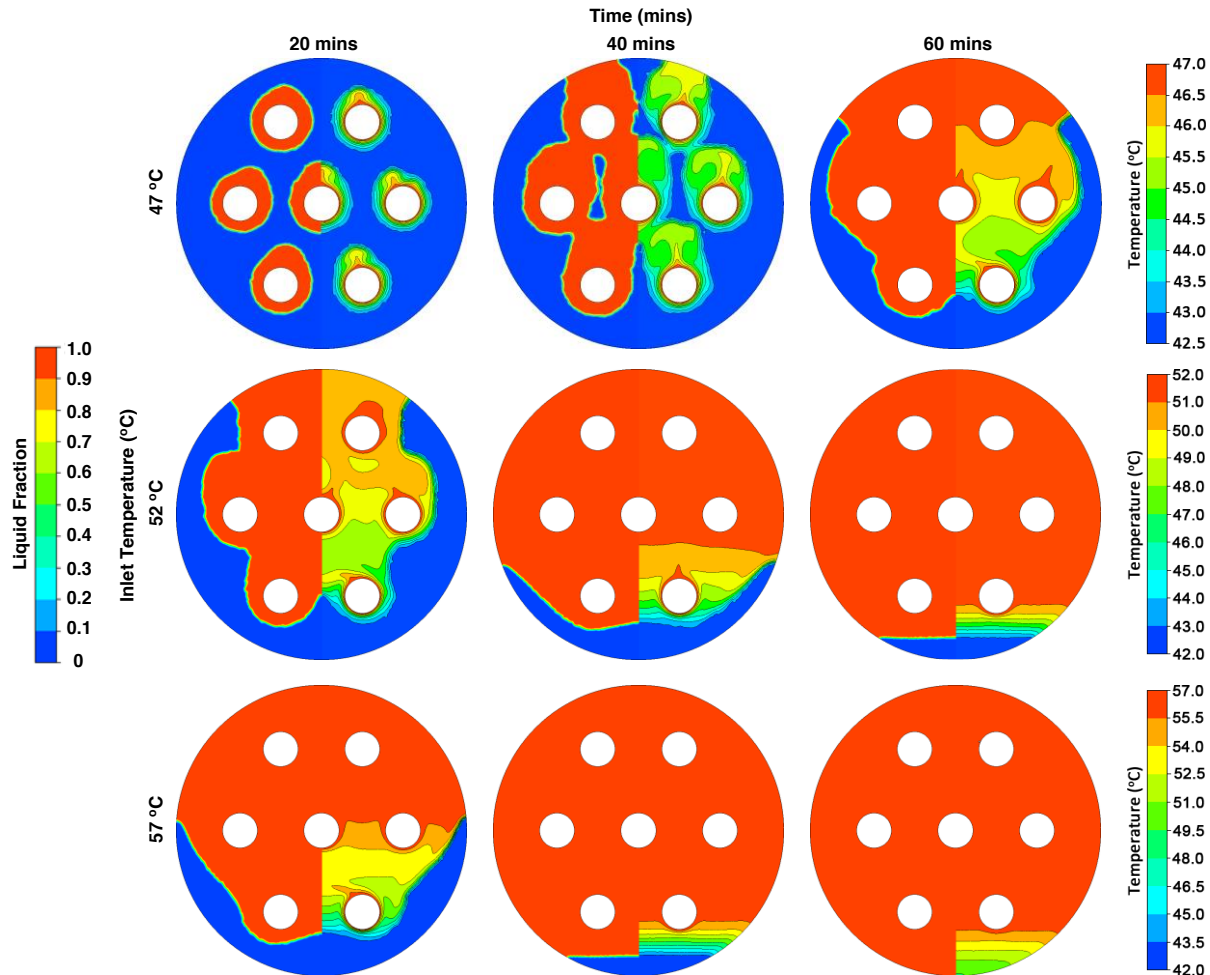


402 **Fig. 7** Transient temperature response of pure paraffin to experimental charging cycles at varied inlet
403 temperatures of 47, 52 and 57 °C and constant volume flow rate of 1.5 l/min.

404 4.1.2 Numerical

405 In numerical simulation, the melting/charging cycles of pure paraffin sample are investigated
406 at three constant inlet temperatures of 47, 52 and 57 °C. As presented in **Fig. 8**, the left side
407 of plots indicates liquid fraction and the right side demonstrates temperature contours of
408 pure paraffin in shell of heat exchanger. It can be observed that as liquid fraction around the
409 HTF tubes increases, the buoyant forces enable liquid particles to rise above and thus, it
410 results in comparatively higher melting rate at top position of shell. Likewise, the temperature
411 contours demonstrate a relatively higher temperature of paraffin at top position as compared
412 to bottom position. Moreover, it is noticed that with an increase in inlet temperature, the
413 melting rate is significantly improved, as shown in **Fig. 8**. It is observed that with an increase
414 in inlet temperature from 47 to 52 and 57 °C, the total melting time is reduced by a fraction of
415 56.96% and 72.60%, respectively. Furthermore, the sensible portion of heat storage in liquid

phase is increased with an increase in inlet temperature, which enhances the overall thermal energy storage of LHS system. It is noticed that with an increase in inlet temperature from 47 to 52 and 57 °C, the overall enthalpy of LHS system is upgraded from 299 to 309 and 319 kJ/kg, respectively.



420

421 **Fig. 8** Liquid fraction and temperature contours of pure paraffin at various inlet temperatures of 47, 52
422 and 57 °C.

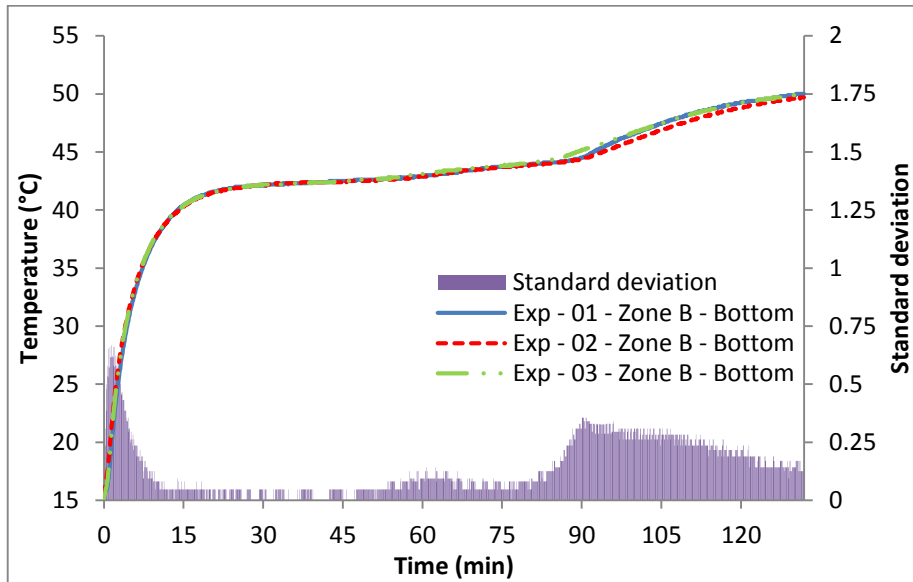
423 4.2 Thermal performance of nano-PCM samples

424 After understanding the thermal behaviour of pure paraffin in shell-and-tube heat exchanger,
425 the experimental and numerical examination of nano-PCM samples are conducted.

426 4.2.1 Experimental

427 As discussed in section 2.1, ultrasonic emulsification technique is adopted to prepare
428 various nano-PCM samples and shell-and-tube heat exchanger is utilised to investigate
429 thermal behaviour of the nano-PCM samples. Thermal conductivity of paraffin improves with
430 an inclusion of nano-additives and thus, the total charging time can be significantly reduced.
431 However, as illustrated in **Fig. 4**, an increase in volume fraction of nano-additives also
432 augments the dynamic viscosity, which has an adverse impact on natural convection and
433 therefore the thermal performance can be affected.

434 To begin with experimental investigations, the repeatability and reliability study of nano-PCM
 435 samples are conducted to examine the consistency of experimental results. For instance,
 436 **Fig. 9** represents the transient temperature profiles acquired while charging Al_2O_3 based
 437 nano-PCM sample with 1% volume fraction at constant inlet temperature of 52 °C. The mean
 438 statistical standard deviation between the transient temperature profiles for three charging
 439 cycles is computed to be 0.138.



440

441 **Fig. 9** Repeatability study of Al_2O_3 based nano-PCM sample with 1% volume fraction while
 442 conducting experimental charging cycles at constant inlet temperature of 52 °C.

443 Following to repeatability tests, three Al_2O_3 based nano-PCM samples are developed with
 444 volume fraction of 1, 3 and 5%. Nano-PCM sample in liquid phase is poured into the shell of
 445 heat exchanger and the experimental investigations are conducted at three varied inlet
 446 temperatures of 47, 52 and 57 °C. The transient temperature profiles for these three Al_2O_3
 447 based nano-PCM samples are recorded by thermocouple installed at bottom position at
 448 zone B and are plotted against pure paraffin in **Fig. 10**.

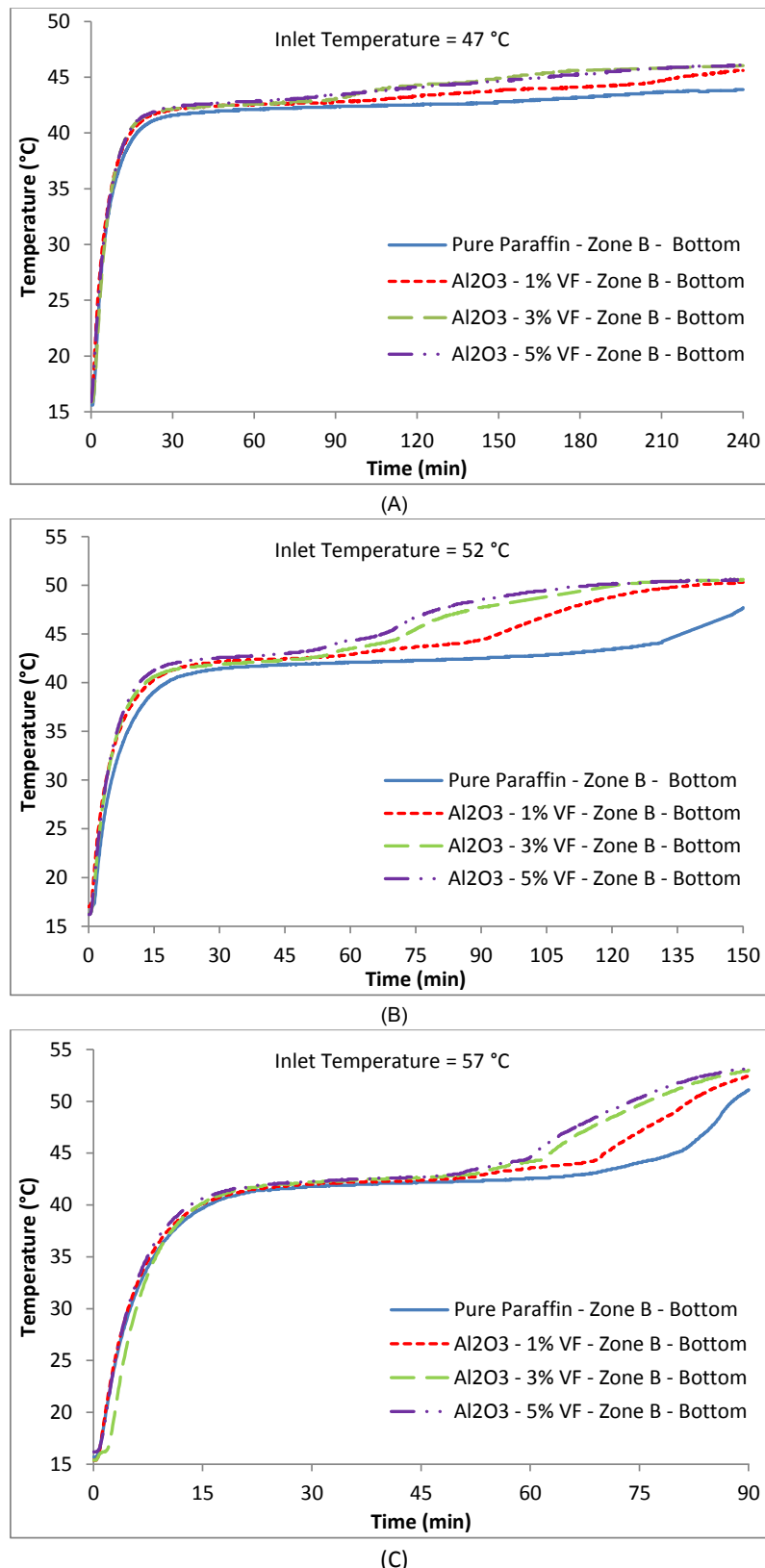
449 It can be noticed that at constant inlet temperature of 47 °C, the melting/charging time at
 450 bottom position is significantly reduced by a fraction 33.75%, 55.41% and 56.25% for Al_2O_3
 451 based nano-PCM samples with volume fraction of 1, 3 and 5% as compared to pure paraffin,
 452 respectively. Likewise, at constant inlet temperature of 52 °C, the charging time is
 453 considerably decreased by a fraction of 35.92%, 48.80% and 56.37%, respectively.
 454 Similarly, in case of constant inlet temperature of 57 °C, the charging time is lessened by a
 455 fraction of 11.36%, 21.71% and 24.74% for Al_2O_3 based nano-PCM samples as compared to
 456 pure paraffin, respectively. It can be noticed that for all three varied inlet temperatures, the
 457 melting/charging time is significantly reduced by incorporating Al_2O_3 based nano-additives to
 458 paraffin. However, with an increase in volume fraction from 3% to 5%, just a slight increment
 459 in thermal performance is observed which is due to adverse effects of higher dynamic
 460 viscosity on natural convection. Therefore, it can be deduced that an optimum volume
 461 fraction is essential to be identified for an appropriate enhancement in thermal performance.

462 Subsequently, the nano-PCM samples based on 1% volume fraction of Al_2O_3 , AlN and GnP
 463 are prepared and experimentally investigated for thermal performance in shell-and-tube heat

464 exchanger at three varied inlet temperatures of 47, 52 and 57 °C. In order to identify the
465 thermal performance enhancement due to inclusion of same volume fraction of varied nano-
466 additives in paraffin, the transient temperature profiles are recorded from thermocouples
467 installed at top and bottom positions at zone A, as presented in **Fig. 11**.

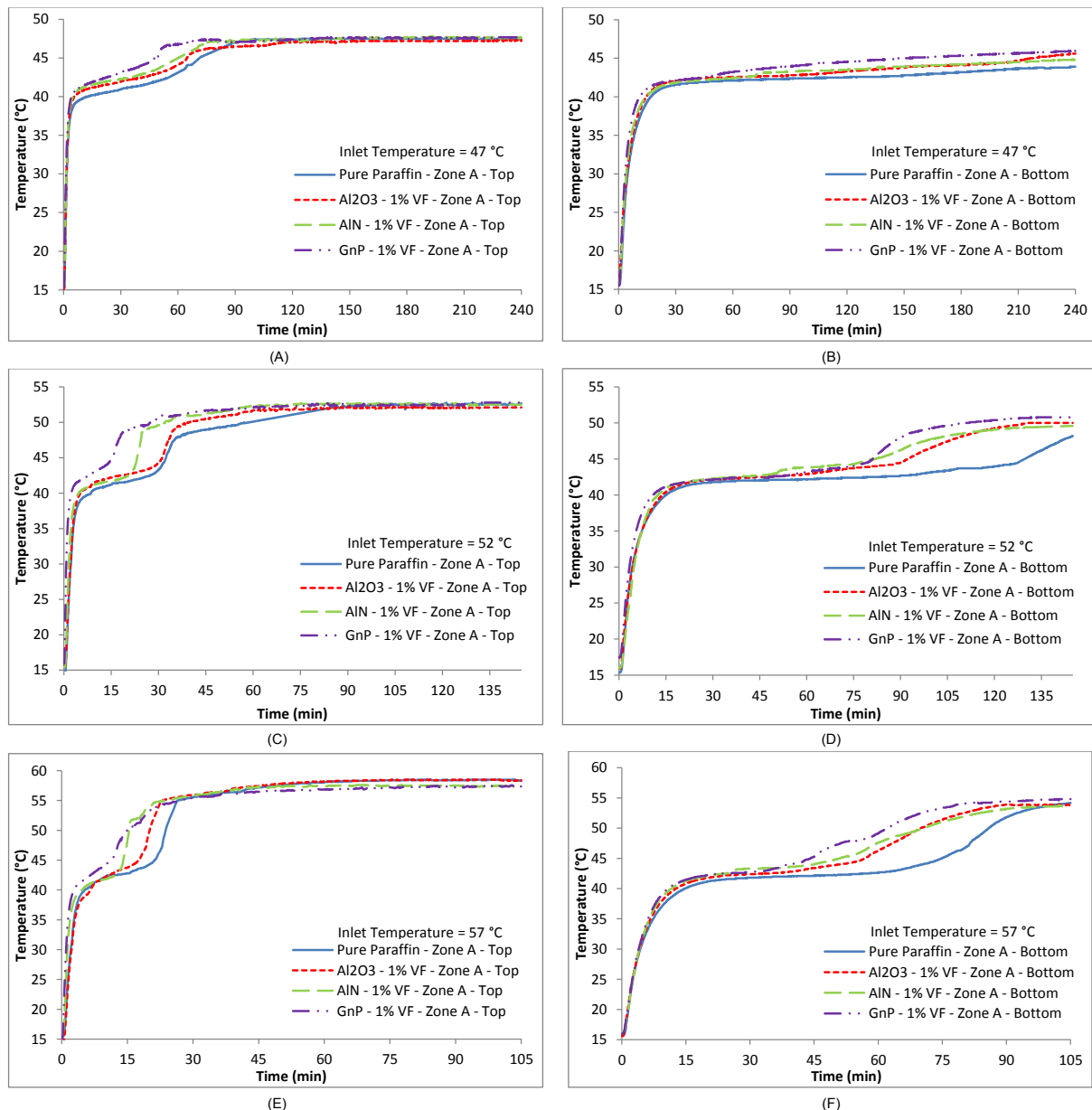
468 It can be observed that at constant inlet temperature of 47 °C, the total melting time at top
469 position for 1% volume fraction of Al₂O₃, AlN and GnP based nano-PCM samples are
470 reduced by a fraction of 9.04%, 18.74% and 37.85% as compared to pure paraffin,
471 respectively. Similarly, the total melting time at bottom position is reduced by a fraction of
472 33.75%, 35.90% and 62.56%, respectively. Moreover, at inlet temperature of 52 °C, the
473 melting time at top position is decreased by 6.42%, 27.27% and 57.22%, respectively.
474 Likewise, at bottom position, the melting time is lessened by 32.70%, 36.40% and 38.07%,
475 respectively. Furthermore, at inlet temperature of 57 °C, the total melting time is decreased
476 by a fraction of 19.04%, 28.57% and 49.78% at top position and 28.01%, 36.47% and
477 44.57% at bottom position, respectively. It can be perceived from experimental results that
478 nano-additives material plays a significant role in enhancing thermal performance of paraffin.
479 For instance, it is noticed that thermal performance enhancement for GnP based nano-PCM
480 sample is relatively higher than Al₂O₃ and AlN based nano-PCM samples due to relatively
481 higher thermal conductivity and smaller particle size of GnP nano-additives.

482 Furthermore, similar to pure paraffin, the variations in volume flow rate of HTF from 1 to 3
483 l/min have presented an insignificant enhancement in charging rate of nano-PCM samples.
484 This is due to small volumetric capacity of shell-and-tube heat exchanger and consequently,
485 the tubes in shell are at same temperature throughout its length.



486

487 **Fig. 10** Transient thermal performance of Al₂O₃ based nano-PCM samples with volume fraction of
 488 1%, 3% and 5% during experimental charging cycles at various inlet temperatures of 47, 52 and 57 °C
 489 and at constant volume flow rate of 1.5 l/min.



490

491 **Fig. 11** Transient temperature plots attained from experimental charging cycles of 1% volume fraction
492 of Al₂O₃, AlN and GnP based nano-PCM samples at varied inlet temperatures of 47, 52 and 57 °C
493 and at constant volume flow rate of 1.5 l/min.

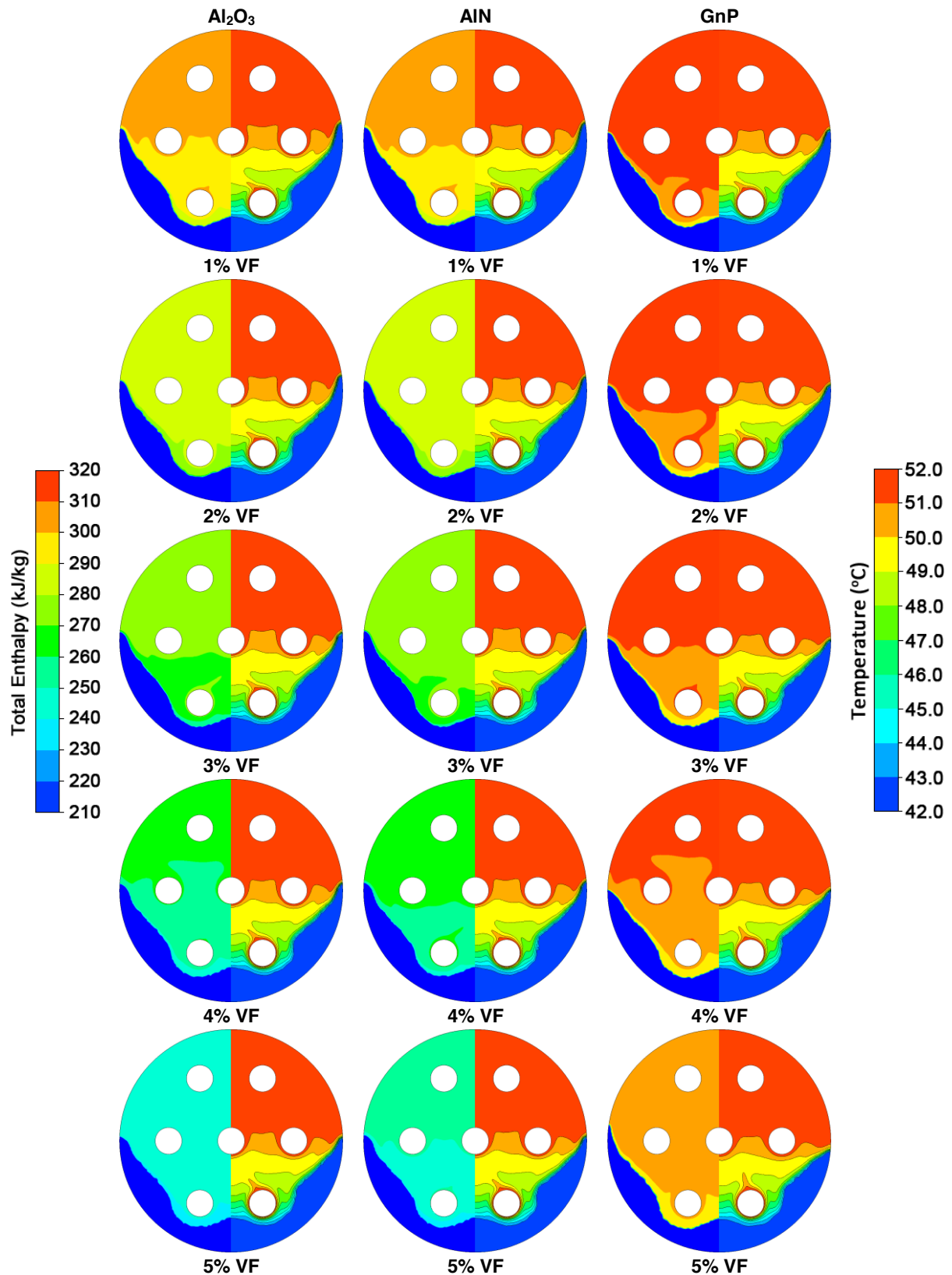
494 4.2.2 Numerical

495 In this section, the numerical simulations of charging cycles of nano-PCM samples based on
496 Al_2O_3 , AlN and GnP nano-additives with volume fraction of 1%, 2%, 3%, 4% and 5% are
497 conducted at constant inlet temperature of 52 °C, respectively. As illustrated in **Fig. 12**, the
498 left sides of plots represent total enthalpy of nano-PCM based LHS system and the right
499 sides demonstrate temperature contours. The plots are attained from simulation results at 30
500 mins of charging cycle.

501 It is observed that temperature contours for Al_2O_3 , AlN and GnP based nano-PCM samples
502 with varied volume fraction represent a small variation in temperature. This is contrary to the
503 fact that GnP based nano-PCM possess higher effective thermal conductivity, as shown in
504 **Fig. 4**. The reason behind is that GnP based nano-PCM also have relatively higher dynamic
505 viscosity which limits the influence of buoyant forces and natural convection on temperature
506 distribution and melting rate. Therefore, the temperature contours are indicating just a slight
507 variation. However, it can be noticed from enthalpy plots that GnP based nano-PCM
508 samples possess significantly higher enthalpy as compared to Al_2O_3 and AlN based nano-
509 PCM samples for all respective volume fraction cases. This is due to the fact that Al_2O_3 and
510 AlN nano-additives have relatively higher density and particle size which considerably
511 reduces the overall thermal capacity and enthalpy of the system.

512 For control volume, the thermal storage capacity is reduced for nano-PCM as compared to
513 pure paraffin because nano-additives occupy certain volume. Therefore, the total enthalpy is
514 reduced for nano-PCM samples. As illustrated in **Fig. 13**, the total enthalpy of nano-PCM
515 samples reduces with an increase in volume fraction of nano-additives as compared to pure
516 paraffin (309 kJ/kg). It is recorded that with an inclusion of 1% volume fraction of Al_2O_3 , AlN
517 and GnP nano-additives, the total enthalpy of system is reduced by a fraction of 4.75%,
518 4.46% and 0.55%, respectively. Likewise, in case of 5% volume fraction of nano-additives,
519 the total enthalpy is decreased by a fraction of 20.58%, 19.64% and 2.88%, respectively. It is
520 noted that due to smaller density and particle size, the GnP based nano-PCM samples have
521 illustrated higher thermal storage capacity as compared to Al_2O_3 and AlN based nano-PCM.
522 Moreover, Al_2O_3 and AlN based nano-PCM have presented higher charging rate as
523 compared to pure paraffin, however the increase in weight and reduction in thermal storage
524 capacity can minimise their utilisation in widespread practical applications.

525

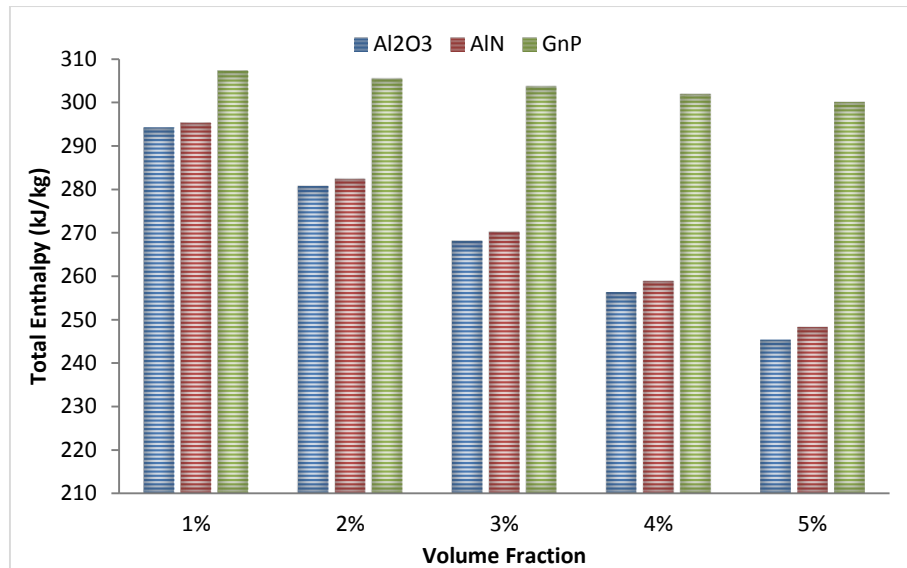


526

527 **Fig. 12** Total enthalpy and temperature contours of Al_2O_3 , AlN and GnP based nano-PCM samples
528 with varied volume fractions attained after 30 mins of charging at constant inlet temperature of 52°C .

529

530



531

532 **Fig. 13** Total enthalpy of nano-PCM samples with varying volume fraction of nano-additives.

533 4.3 Thermal performance of pure paraffin and nano-PCM during discharging cycles

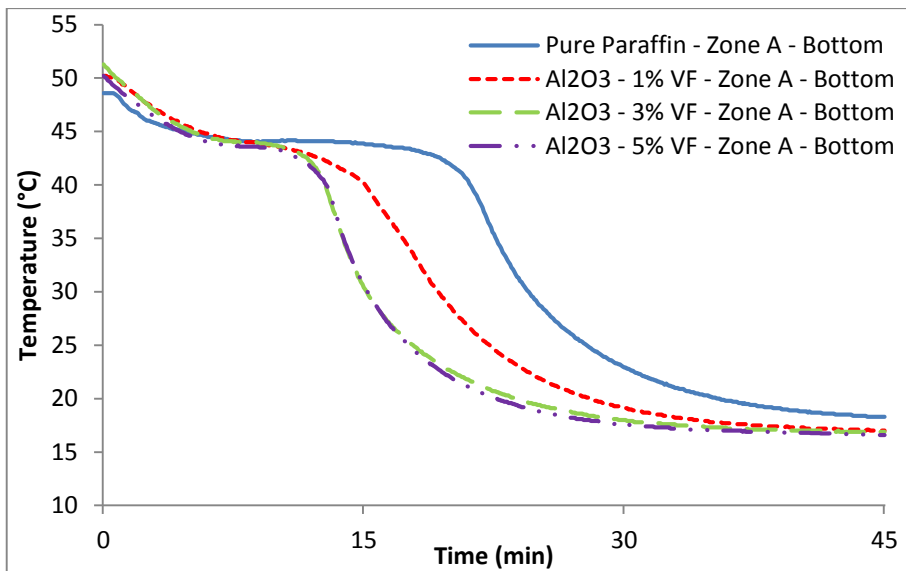
534 After charging cycles, the thermal performance of various samples of nano-PCM in shell-
 535 and-tube heat exchanger are experimentally investigated during discharging cycles.
 536 Municipal water is directed through the tubes of heat exchanger to extract thermal energy
 537 from nano-PCM. In discharging cycles, the inlet temperatures for all cases are set constant
 538 to 15 °C.

539 Due to higher temperature gradient generated between HTF in tubes and nano-PCM in
 540 shell, the sensible portion of thermal energy is rapidly transferred to HTF. As a result, the
 541 temperature of nano-PCM is almost linearly declined to about 44 °C. After this stage, the
 542 discharge of latent portion of thermal energy starts. Due to higher latent heat capacity, the
 543 decrease in temperature from 44 to 41 °C is relatively slow and steady. During this period,
 544 the liquid phase nano-PCM transforms to mushy and then to solid phase. As the latent
 545 portion of thermal energy discharges, a rapid decline in temperature is observed which
 546 represents sensible portion of thermal energy discharge in solid phase.

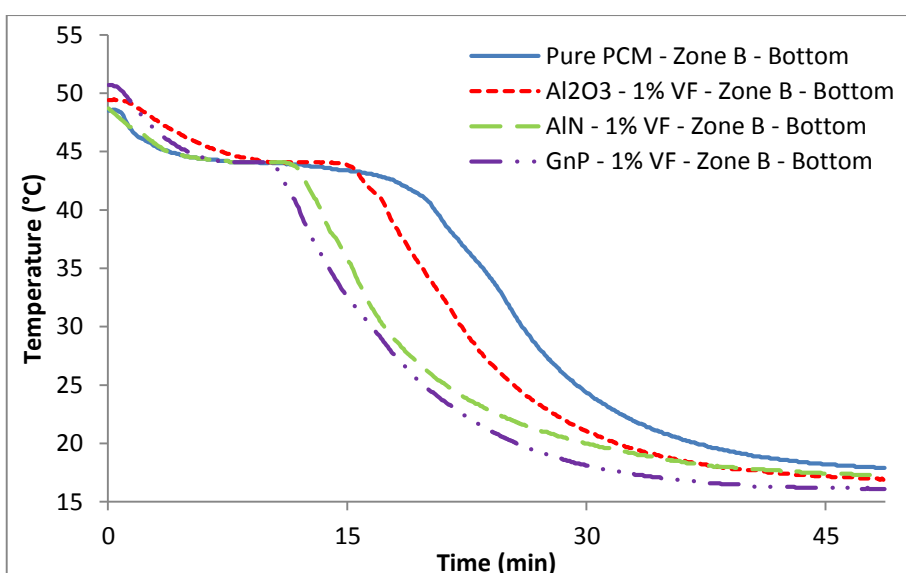
547 Initially, the influence of varying volume fraction of nano-additives on thermal performance
 548 during discharging cycle is examined and plotted against pure paraffin in **Fig. 14**. It can be
 549 noticed that with inclusion of Al_2O_3 nano-additives, the thermal conductivity is enhanced and
 550 therefore, the discharging time is significantly reduced. It is observed that the time required
 551 to discharge latent portion of thermal energy at bottom position at zone A is reduced by a
 552 fraction of 28.45%, 39.05% and 39.52% for Al_2O_3 based nano-PCM samples with volume
 553 fraction of 1%, 3% and 5% as compared to pure paraffin, respectively. Moreover, it can be
 554 noticed that similar to charging cycles, an increase in volume fraction from 3% to 5% has an
 555 insignificant impact on phase transition rate of Al_2O_3 based nano-PCM.

556 Furthermore, in order to examine the impact of varying nano-additives material on thermal
 557 performance, the discharging cycles are experimentally investigated for 1% volume fraction
 558 of Al_2O_3 , AlN and GnP based nano-PCM. The temperature data for nano-PCM samples
 559 registered by thermocouple installed at bottom at zone B are plotted against pure paraffin in
 560 **Fig. 15**. It can be noticed that the discharging time of latent portion of thermal energy is

561 decreased by 14.63%, 34.95% and 41.46% for Al_2O_3 , AlN and GnP based nano-PCM as
 562 compared to pure paraffin, respectively. It can be perceived that due to higher thermal
 563 conductivity of GnP and AlN nano-additives, the discharge rate is significantly higher.



564
 565 **Fig. 14** Transient temperature profiles attained during experimental discharging cycles of pure
 566 paraffin and Al_2O_3 nano-PCM samples of various volume fractions 1%, 3% and 5%. The inlet
 567 temperature of HTF is set to 15 °C for all cases.



568
 569 **Fig. 15** Transient temperature plots acquired during experimental discharging cycles of pure paraffin
 570 and nano-PCM samples of 1% volume fraction of Al_2O_3 , AlN and GnP. The inlet temperature is kept
 571 constant to 15 °C for all cases.

572 5. Conclusions

573 In this article, experimental and numerical studies are conducted to identify the impact of
574 metal oxides, metal nitrides and carbon allotropes based nano-additives on thermal
575 performance enhancement of paraffin based LHS system. Ultrasonic emulsification
576 technique is adopted to prepare Al_2O_3 , AlN and GnP based nano-PCM samples with varied
577 volume fractions. Thermal behaviour of nano-PCM samples are investigated in shell-and-
578 tube heat exchanger by conducting series of charging and discharging cycles at various
579 operating conditions. Meanwhile, a numerical model is developed and simulated to help
580 understand and predict the effect of improved thermal conductivity and dynamic viscosity of
581 nano-PCM samples on heat transfer mechanism, temperature distribution and overall
582 enthalpy of the LHS system. The numerical model accounts for operating temperature,
583 particle size and volume fraction of nano-additives while computing the effective thermal
584 conductivity and dynamic viscosity of nano-PCM samples. Based on experimental and
585 numerical investigations, the following conclusions are derived:

- 586 • It is observed that as the liquid fraction around the tubes increases during charging
587 cycles, an upward rise of high temperature molecules due to buoyant forces enable
588 natural convection to dominate the heat transfer in top position. Therefore, the melting
589 rate is higher at top position as compared to bottom position of the shell-and-tube heat
590 exchanger based LHS system. Likewise, it is noticed that with an increase in inlet
591 temperature of HTF from 47 to 52 and 57 °C, the phase transition rate is significantly
592 improved by a fraction of 56.96% and 72.60%, respectively. Moreover, the overall
593 thermal enthalpy of the system is also improved with an increase in inlet temperature.
- 594
- 595 • It is deduced that the effective thermal conductivity and dynamic viscosity of paraffin is
596 significantly enhanced with inclusion of nano-additives. Likewise, the particle size,
597 volume fraction and operating temperature significantly influence the effective thermal
598 conductivity and dynamic viscosity. The experimental and numerical results indicated
599 that the thermal performance is improved for all nano-PCM samples. However, GnP
600 based nano-PCM samples have illustrated relatively higher effective thermal
601 conductivity and dynamic viscosity due to their smaller particle size and higher thermal
602 conductivity as compared to Al_2O_3 and AlN. It is observed that while charging at inlet
603 temperature of 47 °C, the charging time for Al_2O_3 , AlN and GnP based nano-PCM
604 samples is significantly reduced by 33.75%, 35.90% and 62.56% as compared to pure
605 paraffin. Likewise, for inlet temperature of 52 °C, the charging time is decreased by
606 32.70%, 36.40% and 38.07%, respectively. Similarly, for inlet temperature of 57 °C, the
607 charging time is reduced by 28.01%, 36.47% and 44.57%, respectively. Moreover, the
608 discharging time is also decreased by a fraction of 14.63%, 34.95% and 41.46%,
609 respectively. Therefore, it is concluded that all three nano-additives have presented
610 significant improvement in charging/discharging rate. However, GnP based nano-PCM
611 samples have illustrated relatively better thermal performance.
- 612
- 613 • An optimum volume fraction of nano-additives is critical for an ideal enhancement in
614 thermal performance of LHS system. Al_2O_3 based nano-PCM samples with varying
615 volume fractions of 1%, 3% and 5% are investigated at inlet temperature of 47, 52 and
616 57 °C. In case of inlet temperature of 47 °C, the charging time of Al_2O_3 based nano-
617 PCM samples is significantly reduced by a fraction of 33.75%, 55.41% and 56.25% as

618 compared to pure paraffin. Likewise, in case of inlet temperature of 52 °C, the charging
619 time is decreased by 35.92%, 48.80% and 56.37%, respectively. Also, in case of inlet
620 temperature of 57 °C, the charging time is lessened by 11.36%, 21.71% and 24.74%,
621 respectively. Furthermore, the discharging time is also reduced by a fraction 28.45%,
622 39.05% and 39.52%, respectively. It can be observed that Al₂O₃ based nano-PCM
623 samples have illustrated higher charging and discharging rate. However for all
624 charging/discharging cycles, a minimal enhancement in charging/discharging rate is
625 noticed as the volume fraction of Al₂O₃ is increased from 3% to 5%. Therefore, the
626 optimum volume fraction for Al₂O₃ based nano-PCM samples is identified as 3%.

- 627
- 628 • The inclusion of nano-additives captures certain volume and as a result, it reduces the
629 overall thermal storage capacity of LHS system. It is noticed that with an addition of
630 5% volume fraction of Al₂O₃, AlN and GnP nano-additives, the total enthalpy of LHS
631 system is reduced by 20.58%, 19.64% and 2.88% as compared to pure paraffin. It is
632 noticed that GnP based nano-PCM samples have indicated a slight reduction in
633 thermal storage capacity as compared to Al₂O₃ and AlN based nano-PCM samples.
634 Due to significant reduction in thermal storage capacity and an increase in overall
635 weight of the LHS system, the employability of Al₂O₃ and AlN based nano-PCM
636 samples in large scale practical applications is limited.

637 Acknowledgement

- 638 The authors would like to acknowledge Bournemouth University, UK and National University
639 of Sciences and Technology (NUST), Pakistan for their financial and in-kind support to
640 conduct this research.

641 References

- 642 [1] International Energy Agency (IEA). Energy and Climate Change 21st UN Conference of
643 the Parties (COP21), Paris, 2015.
- 644 [2] S. Suranovic. Fossil fuel addiction and the implications for climate change policy. *Global*
645 *Environmental Change*. 23 (2013) 598-608.
- 646 [3] J.P. da Cunha, P. Eames. Thermal energy storage for low and medium temperature
647 applications using phase change materials—a review. *Applied Energy*. 177 (2016) 227-38.
- 648 [4] A. Sharma, V.V. Tyagi, C. Chen, D. Buddhi. Review on thermal energy storage with
649 phase change materials and applications. *Renewable and Sustainable energy reviews*. 13
650 (2009) 318-45.
- 651 [5] L. Miró, J. Gasia, L.F. Cabeza. Thermal energy storage (TES) for industrial waste heat
652 (IWH) recovery: a review. *Applied Energy*. 179 (2016) 284-301.
- 653 [6] A. Modi, F. Bühler, J.G. Andreasen, F. Haglind. A review of solar energy based heat and
654 power generation systems. *Renewable and Sustainable Energy Reviews*. 67 (2017) 1047-
655 64.
- 656 [7] D. Rabha, P. Muthukumar. Performance studies on a forced convection solar dryer
657 integrated with a paraffin wax-based latent heat storage system. *Solar Energy*. 149 (2017)
658 214-26.
- 659 [8] N. Soares, J. Costa, A. Gaspar, P. Santos. Review of passive PCM latent heat thermal
660 energy storage systems towards buildings' energy efficiency. *Energy and buildings*. 59
661 (2013) 82-103.
- 662 [9] Y. Tian, C.-Y. Zhao. A review of solar collectors and thermal energy storage in solar
663 thermal applications. *Applied Energy*. 104 (2013) 538-53.
- 664 [10] A. Waqas, Z.U. Din. Phase change material (PCM) storage for free cooling of
665 buildings—a review. *Renewable and sustainable energy reviews*. 18 (2013) 607-25.
- 666 [11] L.F. Cabeza, A. Castell, C.d. Barreneche, A. De Gracia, A. Fernández. Materials used
667 as PCM in thermal energy storage in buildings: a review. *Renewable and Sustainable*
668 *Energy Reviews*. 15 (2011) 1675-95.
- 669 [12] Z. Khan, Z.A. Khan. Development in Paraffin Based Thermal Storage System Through
670 Shell and Tubes Heat Exchanger With Vertical Fins. ASME 2017 11th International
671 Conference on Energy Sustainability collocated with the ASME 2017 Power Conference
672 Joint With ICOPE-17, the ASME 2017 15th International Conference on Fuel Cell Science,
673 Engineering and Technology, and the ASME 2017 Nuclear Forum. American Society of
674 Mechanical Engineers2017. pp. V001T11A3-VT11A3.
- 675 [13] N.S. Dhaidan, J. Khodadadi. Melting and convection of phase change materials in
676 different shape containers: A review. *Renewable and Sustainable Energy Reviews*. 43
677 (2015) 449-77.
- 678 [14] Z. Khan, Z. Khan, A. Ghafoor. A review of performance enhancement of PCM based
679 latent heat storage system within the context of materials, thermal stability and compatibility.
680 *Energy Conversion and Management*. 115 (2016) 132-58.
- 681 [15] J. Giro-Paloma, M. Martínez, L.F. Cabeza, A.I. Fernández. Types, methods, techniques,
682 and applications for microencapsulated phase change materials (MPCM): a review.
683 *Renewable and Sustainable Energy Reviews*. 53 (2016) 1059-75.
- 684 [16] J. Khodadadi, L. Fan, H. Babaei. Thermal conductivity enhancement of nanostructure-
685 based colloidal suspensions utilized as phase change materials for thermal energy storage:
686 a review. *Renewable and Sustainable Energy Reviews*. 24 (2013) 418-44.

- [17] L. Liu, D. Su, Y. Tang, G. Fang. Thermal conductivity enhancement of phase change materials for thermal energy storage: A review. *Renewable and Sustainable Energy Reviews*. 62 (2016) 305-17.
- [18] M. Kibria, M. Anisur, M. Mahfuz, R. Saidur, I. Metselaar. A review on thermophysical properties of nanoparticle dispersed phase change materials. *Energy Conversion and Management*. 95 (2015) 69-89.
- [19] M.K. Rathod, J. Banerjee. Thermal performance enhancement of shell and tube Latent Heat Storage Unit using longitudinal fins. *Applied thermal engineering*. 75 (2015) 1084-92.
- [20] A.A.R. Darzi, M. Jourabian, M. Farhadi. Melting and solidification of PCM enhanced by radial conductive fins and nanoparticles in cylindrical annulus. *Energy Conversion and Management*. 118 (2016) 253-63.
- [21] Z. Khan, Z. Khan, K. Tabeshf. Parametric investigations to enhance thermal performance of paraffin through a novel geometrical configuration of shell and tube latent thermal storage system. *Energy Conversion and Management*. 127 (2016) 355-65.
- [22] Z. Khan, Z.A. Khan. An experimental investigation of discharge/solidification cycle of paraffin in novel shell and tube with longitudinal fins based latent heat storage system. *Energy Conversion and Management*. 154 (2017) 157-67.
- [23] Z. Khan, Z.A. Khan. Experimental investigations of charging/melting cycles of paraffin in a novel shell and tube with longitudinal fins based heat storage design solution for domestic and industrial applications. *Applied Energy*. (2017).
- [24] K. Venkitaraj, S. Suresh, B. Praveen, A. Venugopal, S.C. Nair. Pentaerythritol with alumina nano additives for thermal energy storage applications. *Journal of Energy Storage*. 13 (2017) 359-77.
- [25] Y. Tang, D. Su, X. Huang, G. Alva, L. Liu, G. Fang. Synthesis and thermal properties of the MA/HDPE composites with nano-additives as form-stable PCM with improved thermal conductivity. *Applied Energy*. 180 (2016) 116-29.
- [26] S. Harikrishnan, M. Deenadhayalan, S. Kalaiselvam. Experimental investigation of solidification and melting characteristics of composite PCMs for building heating application. *Energy Conversion and Management*. 86 (2014) 864-72.
- [27] J.-N. Shi, M.-D. Ger, Y.-M. Liu, Y.-C. Fan, N.-T. Wen, C.-K. Lin, et al. Improving the thermal conductivity and shape-stabilization of phase change materials using nanographite additives. *Carbon*. 51 (2013) 365-72.
- [28] Z.-T. Yu, X. Fang, L.-W. Fan, X. Wang, Y.-Q. Xiao, Y. Zeng, et al. Increased thermal conductivity of liquid paraffin-based suspensions in the presence of carbon nano-additives of various sizes and shapes. *Carbon*. 53 (2013) 277-85.
- [29] L.-W. Fan, X. Fang, X. Wang, Y. Zeng, Y.-Q. Xiao, Z.-T. Yu, et al. Effects of various carbon nanofillers on the thermal conductivity and energy storage properties of paraffin-based nanocomposite phase change materials. *Applied Energy*. 110 (2013) 163-72.
- [30] Y. Yuan, N. Zhang, T. Li, X. Cao, W. Long. Thermal performance enhancement of palmitic-stearic acid by adding graphene nanoplatelets and expanded graphite for thermal energy storage: A comparative study. *Energy*. 97 (2016) 488-97.
- [31] W. Wang, X. Yang, Y. Fang, J. Ding, J. Yan. Enhanced thermal conductivity and thermal performance of form-stable composite phase change materials by using β -Aluminum nitride. *Applied Energy*. 86 (2009) 1196-200.
- [32] L. Zhang, J. Zhu, W. Zhou, J. Wang, Y. Wang. Characterization of polymethyl methacrylate/polyethylene glycol/aluminum nitride composite as form-stable phase change material prepared by in situ polymerization method. *Thermochimica acta*. 524 (2011) 128-34.

- [33] X. Fang, L.-W. Fan, Q. Ding, X.-L. Yao, Y.-Y. Wu, J.-F. Hou, et al. Thermal energy storage performance of paraffin-based composite phase change materials filled with hexagonal boron nitride nanosheets. *Energy Conversion and Management*. 80 (2014) 103-9.
- [34] Y. Yang, J. Luo, G. Song, Y. Liu, G. Tang. The experimental exploration of nano-Si 3 N 4/paraffin on thermal behavior of phase change materials. *Thermochimica Acta*. 597 (2014) 101-6.
- [35] A.V. Arasu, A.S. Mujumdar. Numerical study on melting of paraffin wax with Al 2 O 3 in a square enclosure. *International Communications in Heat and Mass Transfer*. 39 (2012) 8-16.
- [36] J.M. Mahdi, E.C. Nsofor. Solidification of a PCM with nanoparticles in triplex-tube thermal energy storage system. *Applied Thermal Engineering*. 108 (2016) 596-604.
- [37] Z. Meng, P. Zhang. Experimental and numerical investigation of a tube-in-tank latent thermal energy storage unit using composite PCM. *Applied Energy*. 190 (2017) 524-39.
- [38] N. Das, Y. Takata, M. Kohno, S. Harish. Melting of graphene based phase change nanocomposites in vertical latent heat thermal energy storage unit. *Applied Thermal Engineering*. 107 (2016) 101-13.
- [39] T.-P. Teng, Y.-H. Hung, T.-C. Teng, H.-E. Mo, H.-G. Hsu. The effect of alumina/water nanofluid particle size on thermal conductivity. *Applied Thermal Engineering*. 30 (2010) 2213-8.
- [40] D.D. Gray, A. Giorgini. The validity of the Boussinesq approximation for liquids and gases. *International Journal of Heat and Mass Transfer*. 19 (1976) 545-51.
- [41] D.A. Nield, A. Bejan, Nield-Bejan... *Convection in porous media*. Springer2006.
- [42] L.-W. Fan, Z.-Q. Zhu, Y. Zeng, Q. Lu, Z.-T. Yu. Heat transfer during melting of graphene-based composite phase change materials heated from below. *International Journal of Heat and Mass Transfer*. 79 (2014) 94-104.
- [43] M. Corcione. Empirical correlating equations for predicting the effective thermal conductivity and dynamic viscosity of nanofluids. *Energy Conversion and Management*. 52 (2011) 789-93.
- [44] A. Einstein. Eine neue bestimmung der moleküldimensionen. *Annalen der Physik*. 324 (1906) 289-306.
- [45] H. De Bruijn. The viscosity of suspensions of spherical particles.(The fundamental η -c and ϕ relations). *Recueil des travaux chimiques des Pays-Bas*. 61 (1942) 863-74.
- [46] H. Brinkman. The viscosity of concentrated suspensions and solutions. *The Journal of Chemical Physics*. 20 (1952) 571-.
- [47] I.M. Krieger, T.J. Dougherty. A mechanism for non-Newtonian flow in suspensions of rigid spheres. *Transactions of the Society of Rheology*. 3 (1959) 137-52.
- [48] G. Batchelor. The effect of Brownian motion on the bulk stress in a suspension of spherical particles. *Journal of fluid mechanics*. 83 (1977) 97-117.
- [49] J.C. Maxwell. *A treatise on electricity and magnetism*. Clarendon press1881.
- [50] V.D. Bruggeman. Berechnung verschiedener physikalischer Konstanten von heterogenen Substanzen. I. Dielektrizitätskonstanten und Leitfähigkeiten der Mischkörper aus isotropen Substanzen. *Annalen der physik*. 416 (1935) 636-64.
- [51] R. Hamilton, O. Crosser. Thermal conductivity of heterogeneous two-component systems. *Industrial & Engineering chemistry fundamentals*. 1 (1962) 187-91.
- [52] Y. Xuan, Q. Li, W. Hu. Aggregation structure and thermal conductivity of nanofluids. *AIChE Journal*. 49 (2003) 1038-43.

780 [53] R. Kandasamy, X.-Q. Wang, A.S. Mujumdar. Transient cooling of electronics using
781 phase change material (PCM)-based heat sinks. Applied Thermal Engineering. 28 (2008)
782 1047-57.

783